CHALMERS
UNIVERSITY OF TECHNOLOGY

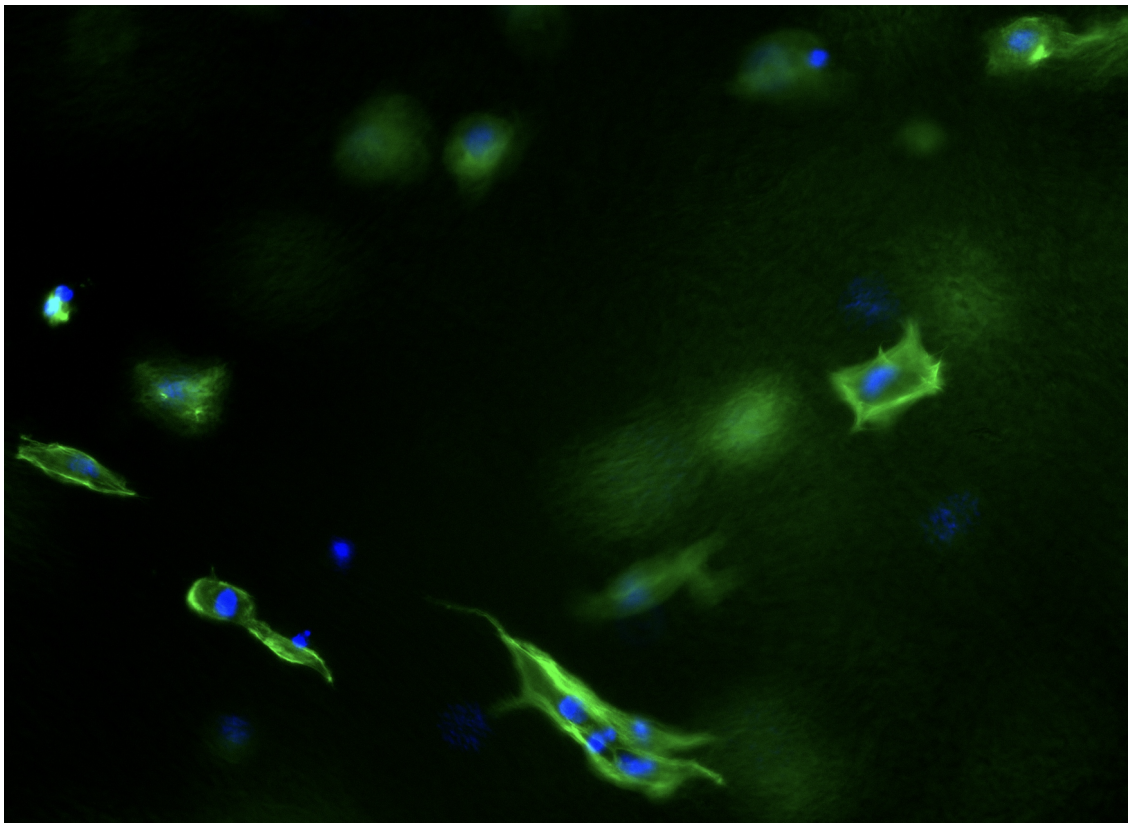

The influence of viscoelastic properties of bioinks on 3D bioprinted tissue models

A study of cell behaviour and printability

Master's thesis in Master's Programme Biotechnology

SOFIE EKSTRÖM

DEPARTMENT OF PHYSICS
CHALMERS UNIVERSITY OF TECHNOLOGY
Gothenburg, Sweden 2023
www.chalmers.se

Master's thesis 2023

The influence of viscoelastic properties of bioinks on 3D bioprinted tissue models

A study of cell behaviour and printability

SOFIE EKSTRÖM

CHALMERS
UNIVERSITY OF TECHNOLOGY

Department of Physics
Chalmers University of Technology
Gothenburg, Sweden 2023

The influence of viscoelastic properties of bioinks on 3D bioprinted tissue models
A study of cell behaviour and printability
SOFIE EKSTRÖM

Supervisor: Elin Pernevik, CELLINK Bioprinting AB
Examiner: Julie Gold, Department of Physics

Master's Thesis 2023
Department of Physics
Chalmers University of Technology
SE-412 96 Gothenburg
Telephone +46 31 772 1000

Cover: MSCs in a 3D bioprinted construct of GelXA. The green fluorescence is visualizing the F-actin and the blue fluorescence the nuclei of the cells. The image is also included in Figure 4.10 where more details can be found.

Typeset in LaTeX
Printed by Chalmers Reproservice
Gothenburg, Sweden 2023

The influence of viscoelastic properties of bioinks on 3D bioprinted tissue models
A study of cell behaviour and printability
SOIFE EKSTRÖM
Department of Physics
Chalmers University of Technology

Abstract

The recent advancement within the field of 3D bioprinting has enabled its application in areas such as the pharmaceutical industry, tissue engineering and many types of cell-based research. The principle is to utilize 3D printing technology to print a variety of biomaterials together with viable cells, to produce accurate tissue models by mimicking the in vivo cell environment. Bioinks used for 3D bioprinting are commonly composed of hydrogels based on naturally derived polymers like gelatin, collagen, alginate and nanofibrillated cellulose (NFC). Bioinks are viscoelastic materials which can be crosslinked after being printed to keep their structure and shape. The crosslinking method and conditions determine the stiffness of the resulting tissue construct, which can in turn also affect the behaviour of incorporated cells. This study aims to investigate the influence of the bioink's viscoelastic properties on both cell behaviour and printability of the bionink. The studied bioinks include CELLINK Bioink, GelMA, GelMA C, GelXA and Photogel95, which are crosslinked either ionically using a $CaCl_2$ solution or using photo-crosslinking, or a combination of the two.

The bioinks' viscoelastic properties, as well as stiffness after crosslinking at two different conditions for each bioink were investigated using rheological measurements, showing that different stiffnesses could be achieved. 3D bioprinting of the bioinks with mesenchymal stem cells (MSC) was used to produce samples which were crosslinked at the same two conditions, cultured over 14 days and analyzed at several time points. The cell viability was evaluated by fluorescent staining using Calcein-AM and propidium iodide (PI), and the cell morphology by using Actin-Green and DAPI, followed by fluorescent microscopy imaging. The stiffness of the cell samples over time was also evaluated by measurements at the same time points.

The stiffness of the cell samples over time showed some unexpected results and high variation between samples, which can to some extent be explained by the method not being fully suitable and well-adapted for these samples. The cell viability was relatively high at day 1 for all bioinks and crosslinking conditions, above 90 % for most samples but around 80 % for a few. A decrease in cell viability was then observed for all samples at day 7 and day 14. The cell morphology analysis showed cells spreading in all gelMA-based bioinks at day 7 and day 14, except for Photogel95. However, no distinct correlations between the stiffnesses achieved at the different crosslinking conditions and the cell behaviour could be determined.

Keywords: 3D bioprinting, bioinks, viscoelastic properties, rheology, MSC.

Acknowledgements

I would firstly like to thank my very enthusiastic and supportive supervisor Elin Pernevik who has guided me through this project, training me in the lab and helping me understand all important concepts. I have really appreciated your patience and pedagogic explanations to all my questions, which there have been many of. I would also like to thank everyone in the SAPPS team at CELLINK for the warm welcome and for sharing your broad knowledge, providing me with great feedback and suggestions on my project. It has been inspiring to get a glimpse of your work and I am grateful for getting the chance to do my Master's Thesis in your group. Lastly, I also want to thank my engaged examiner Julie Gold for showing great interest in my project and supporting me from start to finish.

Sofie Ekström, Gothenburg, June 2023

List of Acronyms

Below is a list of acronyms that have been used throughout this Master's Thesis, in alphabetical order:

3D	Three-dimensional
DAPI	4',6-diamidino-2-phenylindol
DMEM	Dulbecco's modified eagle medium
FBS	Fetal bovine serum
FITC	Fluorescein isothiocyanate
HBSS	Hanks' balanced salt solution
LAF	Laminar air flow
LAP	Lithium phenyl-2,4,6-trimethylbenzoylphosphinate
LVE	Linear viscoelastic region
MA	Methacrylate
MSC	Mesenchymal stem cell
NFC	Nanofibrillated cellulose
PBS	Phosphate buffered saline
RGD	Arginine-glycine-aspartic acid
TXRED	Texas Red
UPP	Upper peltier plate
UV	Ultraviolet

Contents

List of Figures

List of Tables

1
Introduction

Within the biomedical and pharmaceutical industry, the ethical concerns regarding animal testing are an important factor in the transformation of conventional methods and the development of future, more sustainable and relevant approaches for cell and tissue-based research. Although the EU has had a legislation for the protection of animals used for experimental and other scientific purposes since 1986, it was not until 2010 that the principle of the "Three R's", replacement, reduction, and refinement, was incorporated as a legal requirement to be considered [1]. Animals are nevertheless being used in several areas such as in drug testing for drug development and sometimes as donors for tissue and organ transplantation. Moreover, it has been estimated that the process of developing a novel drug takes about 10 to 15 years and cost over 1 billion US dollars before it reaches the market [2]. On average, 17 people also die every day due to organ shortage [3]. This makes it evident that there is a need for more effective drug development, more accurate experimental models as well as more alternatives for organ transplantation.

The advancement within the field of three-dimensional (3D) bioprinting has enabled a means of generating living tissues and organs in the laboratory for applications in areas such as the pharmaceutical industry, drug screening, tissue engineering, regenerative medicine, and cancer research. The principle of 3D bioprinting is to utilize 3D printing technology to print a variety of biomaterials together with viable cells. Unlike conventional methods for synthesizing biomaterials, 3D bioprinting can produce more accurate tissue constructs and models in a high-throughput manner. The controlled architecture can facilitate e.g., controlled delivery of drugs and growth factors, and also allows co-culturing of different cell types in the engineered tissue constructs. [4]

CELLINK Bioprinting is a company with a large portfolio of bioinks and 3D bioprinters, with customers ranging from academia primarily, to pharma, and therefore desires printing all types of tissue models. There are already many internal application notes in addition to customer data using CELLINK products, but due to the bioinks being treated and used slightly different in many cases, a comprehensive understanding of how variation in factors such as crosslinking method and parameters affects printability, stiffness and cell behaviour is missing. Investigating this issue and providing valuable knowledge would allow CELLINK to offer more specific recommendations to customers through their Bioprinting protocols on how to generate printed models with specific biomechanical properties and printing fidelity, as well as its impact on cell behaviour.

1.1 Aim

The overall aim of the project is to investigate the influence of viscoelastic properties of bioinks on cell behaviour and printability in 3D bioprinted tissue models. This will be investigated for different bioinks and varying crosslinking methods and parameters. The aim is to evaluate the cell behaviour by analyzing cell viability and cell morphology in 3D bioprinted constructs.

The aim is further specified by the following questions:

- What conditions are appropriate for 3D bioprinting with the evaluated bioinks to achieve good printability?
- What range of stiffnesses can be achieved for the evaluated bioinks with the different crosslinking methods and conditions?
- What stiffnesses are measured for 3D bioprinted samples with cells?
- How is the cell viability and cell morphology affected by different stiffnesses of the bioinks?

The investigated bioinks include CELLINK Bioink, GelMA, GelMA C, GelXA and Photogel95, which are all products of CELLINK Bioprinting AB. The crosslinking methods evaluated are ionic crosslinking using a $CaCl_2$ solution and photocrosslinking using light at 405 nm.

1.2 Limitations

The general limitations of the project are that only extrusion-based pneumatic 3D bioprinting will be used, together with the presented bioinks. For crosslinking, specified methods and parameters will be tested for each of the bioinks. For evaluation of cell behaviour in the printed constructs, only MSCs will be used and studied in proliferation media. No differentiation studies are included. With regards to viscoelastic properties of the bioinks, rheological measurements will be limited to measuring the storage and loss modulus of the bioinks.

2
Theory

In this chapter, the theory relevant for the different parts of the project is described and explained.

2.1 3D bioprinting

The outcome and quality of 3D bioprinting mainly depends on the efficiency of the 3D bioprinter and the so-called bioink and its properties [4]. There are several different 3D bioprinting techniques, divided as either based on laser-induced forward transfer, inkjet printing or robotic dispensing. Due to its ability to fabricate constructs of relevant sizes within a realistic time frame for the desired applications, robotic dispensing is generally considered as the most promising one. Using this technique, the bioink is usually extruded through the nozzle of a plastic syringe with pressure that is either pneumatic, piston- or screw-driven [5].

2.2 Bioinks

There are many requirements on bioinks to be used in 3D bioprinting as they both need to be compatible with the 3D bioprinter to achieve good printability, and facilitate a suitable environment for viable cells. The general properties of bioinks are described in this section, followed by a more detailed description of the bioinks used in this project in the next section.

2.2.1 Biomaterials used in bioinks

Bioinks are commonly composed of hydrogels since the high-water content makes them suitable for incorporation of cells and bioactive compounds by simulating a 3D environment similar to the natural extracellular matrix (ECM). Commonly used hydrogels, which are based on naturally derived polymers, are gelatine, collagen, alginate, chitosan, and hyaluronic acid. For a bioink to function successfully in bioprinting, it is important that both its physical and biological properties are adequate. With regards to printability, a hydrogel with relatively high polymer concentration, viscosity and stiffness is desired for the construct to maintain its imposed shape. On the other hand, cells thrive in more aqueous environments where migration is not restricted by a dense polymer network. The possible "biofabrication window" therefore lies somewhere in-between these two states. [5]

2.2.2 Crosslinking of bioinks

For a hydrogel construct to keep its shape and structure after printing, some sort of gelation is necessary. This can either be physical gelation based on reversible interactions or chemical gelation based on the formation of covalent bonds, or a combination of the two [5]. Physical gelation, also called physical crosslinking, often includes polymer entanglement or ionic interactions which mainly depend on the intrinsic properties of the polymer. This limits the possibility to control and fine-tune physical crosslinking, but it does not require modification of the polymer chains and is usually easily reversible if necessary. For nature-derived polymers, e.g., from seaweed or of animal origin, gelation is usually thermally driven. With a change in temperature, physical entanglement of the polymer and formation of packed polymer chains occurs because of a shift in their solubility [6].

Molecular self-assembly is another physical crosslinking alternative, which is especially common for protein-based hydrogels such as collagen. By weak non-covalent bonding mechanisms, the collagen protein sequences are folded into hierarchical structures making up the collagen fibres in the hydrogel. Since many natural polymers are negatively charged, physical crosslinking can also occur due to electrostatic interactions or chelation. The presence of divalent cations, e.g., Ca^{2+} or Ba^{2+}, makes negatively charged alginate polymers gel in an "egg-box" pattern where the polymer chains surround ions which are locked in-between as illustrated in Figure 2.1. [6].

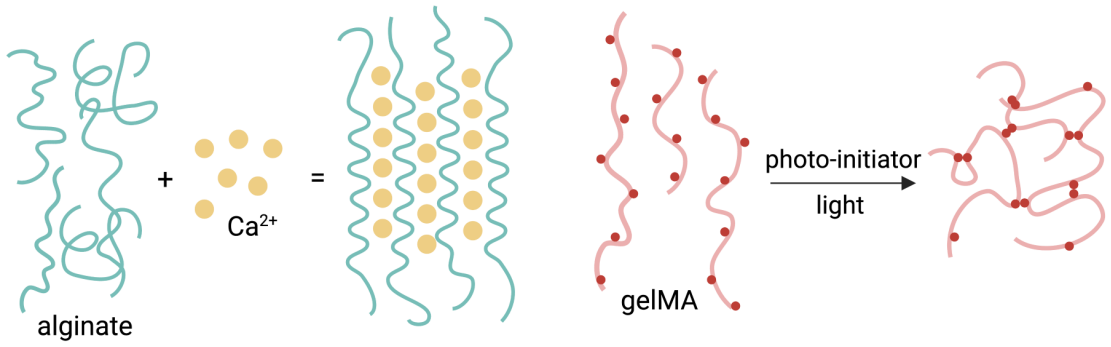

Figure 2.1: Ionic crosslinking of alginate using Ca^{2+} ions (left) and photo-crosslinking of gelMA using a photo-initiator and light (right). Image created in BioRender.

Chemical crosslinking techniques enable more control and precise management of the crosslinking procedure, including both spatial and temporal flexibility. By coupling chemically active molecules or components to the polymer backbone or side chains, covalent bonds can form and create a gel [6]. Chemical crosslinking is mainly used in post-processing for stabilizing weak, physically crosslinked printed constructs. An example is gelMA, a gelatin hydrogel with methacrylate (MA) groups attached along the polymer chains, which is printed warm and undergoes physical crosslinking upon cooling. Subsequent photo-curing can be used to initiate a reaction between the MA groups and stabilize the construct chemically, illustrated in Figure 2.1. However, ultraviolet (UV) light can have harmful effects on cells incorporated in the bioink, which must be considered when using this approach [5].

2.2.3 Rheological properties of bioinks

The printability of a bioink is largely affected by rheological properties during printing, in this case referring to the impact on flow of matter under application of external forces. Viscosity is described as the resistance of a fluid to flow upon the application of stress, and it directly influences the shape fidelity of deposited structures. High viscosity generally increases printing fidelity, but also results in an increase in applied shear stress, which may harm the cells in the bioink. Polymer concentration and the polymer molecular weight are the main contributors to the viscosity, but the solubility parameter, shear rate and temperature also have an influence. [5]

Another essential rheological property is shear thinning, which means a decrease in viscosity at increased shear rate. When shear is applied, the polymer chains are reorganized into a more stretched out conformation with less entanglements and therefore leading to lower viscosity. The shear thinning behaviour is observed primarily for hydrogels with polymers of high molecular weight, but in some extent for most polymeric systems. In the bioprinting process, this leads to the bioink having a lower viscosity inside the printing nozzle where the shear rate is high, followed by an increase in viscosity upon deposition outside of the nozzle, as illustrated in Figure 2.2. This can contribute to a higher printing fidelity. [5]

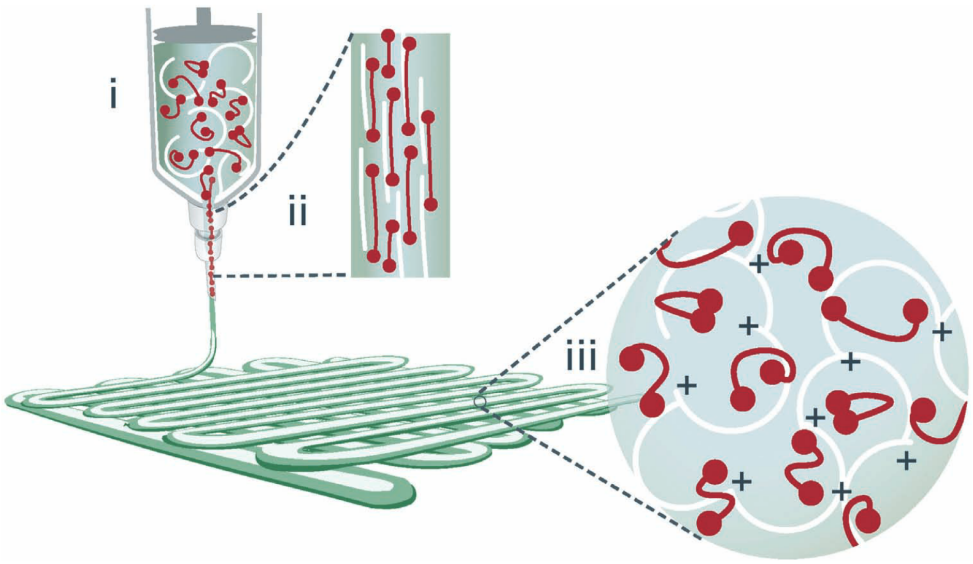

Figure 2.2: Illustration of a shear thinning bioink being extruded through a nozzle during 3D bioprinting. In step (i) entangled polymer chains can be observed, while a more stretched out polymer conformation is observed in step (ii) as a result of the occurring shear. In step (iii), the polymer chains do not experience any shear, and therefore return to their initial conformation and subsequently regain a higher viscosity. Image reproduced from Malda *et al.* (2013) [5], with permission from the author.

2.2.4 Viscoelastic properties of bioinks

Viscoelastic materials are materials that show both elastic and viscous behaviour at the same time. The elastic behaviour is represented by storage modulus, denoted G', and is a measure of the deformation energy stored by the sample during a shear process. If a material is storing the whole deformation energy applied by shear, it will show completely reversible deformation behaviour and stay unchanged in shape after a load cycle. The viscous behaviour is represented by loss modulus, denoted G", and is a measure of the deformation energy used up by the sample during a shear process. Completely viscous materials with irreversible deformation behaviour will change in shape after a load cycle. The energy that is lost is used in the process of changing the material's structure, i.e. when the sample is flowing. The flow in this case refers to the relative motion between the molecules, particles or other components in the material. The frictional forces between these components lead to frictional heat occurring, of which some will heat up the sample and some will be lost to the surrounding environment. [7]

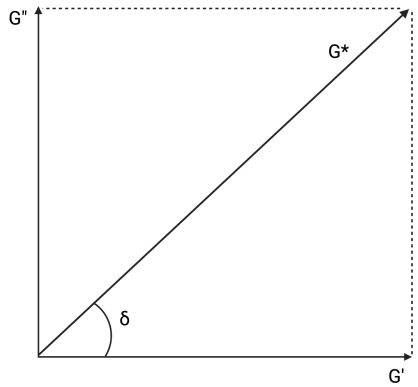

Figure 2.3: Storage modulus (G'), loss modulus (G") and resulting vector complex modulus (G^*). The loss factor, tan δ, is the ratio of the loss modulus and the storage modulus.

The resulting vector of the storage and loss modulus, seen in Figure 2.3, is the complex modulus, denoted G^*. The loss factor, tan δ, is defined as the quotient of the lost and stored deformation energy, i.e., the ratio of the loss modulus and the storage modulus. A value of tan $\delta > 1$ means a fluid or liquid state of the material ("sol state"), and a value of tan $\delta < 1$ means a more gel-like or solid state. The state in-between, called the sol/gel transition point, occurs when $\delta = 1$. [7]. This state is utilized in 3D bioprinting where it is also called crossover temperature, which can be translated as the "printing temperature" of the bioink, where the viscoelastic properties are appropriate for printing.

2.2.5 Biological properties of bioinks

As previously mentioned, the biological properties of the bioink are essential for facilitating an appropriate cell environment. Since the bioink is in direct contact with the cells, resembling the natural ECM, it needs to maintain the cells' viability

and support their adhesion, growth, proliferation, and differentiation. However, one bioink cannot support growth and viability of all cell types as specific properties are required for e.g., soft, and hard tissues. Bioinks can fortunately be tuned by various strategies in the hydrogel formation process, such as mixing with other materials, using different concentrations and special reinforcement agents, as well as crosslinking after printing. [4]

Cells constantly sense their surrounding milieu and make decisions of their fate through cell-ECM interactions via cell membrane-bound receptors. Signals from the ECM, or the bioink in the case of a printed tissue construct, initiate intracellular signalling cascades which are converted into cellular responses. In turn, the cells also exert forces on the bioink scaffolds, which makes understanding this interplay between cells and their surroundings fundamental for successfully mimicking desired tissue properties [8]. The ECM consists of a complex combination of structural and adhesive proteins, such as collagen, elastin, fibronectin, and laminin. These can have different domains for binding to cell surface receptors, often integrins, but also share common structural motifs like arginine-glycine-aspartic acid (RGD) which is an essential motif for many cell-ECM interactions [9]. The extracellular substrate stiffness affects both stem cells and mature cells in the three steps mechanosensation, mechanotransduction and downstream mechanoresponse. It influences the cells' differentiation, proliferation, and morphology [8].

2.3 Bioinks used in this study

The bioinks which were investigated in the project, and their main components, are listed in Table 2.1. All bioinks are products from CELLINK Bioprinting AB where this project was performed. CELLINK Bioink and GelXA are the only bioinks which contain alginate, meaning that they can be ionically crosslinked. GelMA, GelMA C, GelXA and Photogel95 all contain methacrylated gelatin (gelMA) and photoinitiator lithium phenyl-2,4,6-trimethylbenzoylphosphinate (LAP), which makes them photocrosslinkable (photoX). The concentration of LAP is 0.25 % (w/v) in all bioinks.

Table 2.1: The investigated bioinks and their main components.

Bioink	**Components**
CELLINK Bioink	Alginate, NFC
GelMA	gelMA (50% MA), LAP
GelMA C	gelMA (50% MA), LAP, NFC
GelXA	gelMA (50% MA), LAP, xanthan gum, alginate
Photogel95	gelMA (95% MA), LAP

Alginate is a polysaccharide that can be extracted from several types of brown algae [10] which is widely used in biomedical applications, including 3D bioprinting as a cell carrier scaffold [11]. Depending on the source of alginate, it can have very different composition of monomer units which affects its properties [12]. Before

crosslinking, alginate generally behaves as a shear thinning material with low viscosity, meaning that it often needs to be stabilized by a thickening agent to facilitate extrusion into filaments that retain their shape [11]. Since alginate lacks mammalian cell-adhesive properties, addition of biologically active ligands are important to promote and regulate cellular interaction for application in tissue engineering. The biodegradability of alginate is dependent on the enzyme alginase, not present in mammals, which needs to be considered if using alginate for implantation in the human body. By modification of the alginate chains the biodegradability can be improved, but this needs to be investigated for the specific alginate type used for a certain application [12].

Nanocelluloses are a group of renewable nanomaterials frequently used in bioink formulation as they exhibit appropriate rheological properties and structural features that can provide support similar to the ECM. Nanofibrillated cellulose (NFC) is produced from biomass, such as wood pulp, to obtain fibrils with diameters of 5-60 nm and lengths up to roughly a micrometer. Due to the high aspect ratio, NFC gives a gel-like consistency in aqueous solutions above a certain concentration, specific for each NFC variant. The viscosity of NFC-based bioinks can be increased rapidly with increasing concentration, but even at lower concentrations of around 1 wt%, the hydrogel is stable with a strong viscoelastic modulus. The printability of NFC in extrusion-based 3D bioprinting is supported by the shear thinning properties of the hydrogel, and the fibrous structure is somehow analogous to collagen and fibronectin of the native ECM. There is currently medical-grade NFC commercially available to be used as a generic 3D cell culture matrix or to be mixed with other components to further optimize the cell-interactions [13].

Xanthan gum is an extracellular polymer which is produced through aerobic fermentation in *Xanthomonas campestris* bacteria. It is widely used in the food industry as a thickener and stabilizing agent, in the pharmaceutical industry for e.g., drug delivery and in tissue engineering. It shows high stability under a wide range of temperatures and pH-levels and has a high viscosity at low concentrations. It has good biodegradability and is non-toxic, making it suitable for biomedical applications [14].

Gelatin is another well-studied protein for application within 3D bioprinting. It is extracted from animal-derived collagen through hydrolysis and can be dissolved in water solutions to create a hydrogel. It is a non-toxic and non-immunogenic polymer which can facilitate cell adhesion via natural cell binding motifs like RGD. The chemical structure and biological functions of gelatin resembles the ones of collagen, which is found in the native ECM, and promotes the proliferation and differentiation of cells. In its natural form gelatin has low mechanical and thermal properties, becoming a liquid solution at 37 °C, degrading relatively quickly and showing no long-term mechanical stability. For cell culture in gelatin models, at 37 °C, and for development of tissue models for medical applications, this is a drawback. However, the mechanical and thermal properties can be improved by modification of the gelatin polymer and subsequent crosslinking. Several options for modifying the functional groups have been developed, where coupling with methacrylic anhydride

(MA) is one of the most widely used. The resulting gelMA polymer is similar to pure gelatin with regards to degradation, thermal properties and biological properties, but can generate a stable hydrogel at 37 °C via crosslinking [15].

To crosslink gelMA using photo-crosslinking, there are different photo-initiators available, e.g., TiO_2, Irgacure 2959 and LAP [15], which was used in this project. The effect of the photo-initiator on the cells incorporated in the bioink, is something which has been investigated in different studies. In one by Xu *et al.* [16], the effect of both Igracure 2959 and LAP was tested on fibroblasts in a gelMA-based bioink which was photo-cured using light of 365 nm. The cell viability was evaluated using a fluorescent assay which showed that the cell viability generally decreased with an increase in photo-initiator concentration and printing time for both Igracure 2959 and LAP. At low photo-initiator concentrations (0.3 % and 0.5 % (w/v)), the overall cell viability was good for a printing time of 60 min for both Igracure 2959 and LAP, but a higher photo-initiator concentrations (0.7 % and 0.9 % (w/v)) the overall cell viability was higher when using LAP compared to when using Igracure 2959. The post-printing cell viability was analyzed after 24 hours for a concentration of 0.3 % (w/v) photo-initiator, with crosslinking for 45 s using UV light (365 nm) after printing for 15 min. For both Igracure 2959 and LAP, the viability was maintained at around 80 %.

As the light used during photo-crosslinking can have a negative effect on the incorporated cells, the wavelength used for different photo-initiators is something that also should be considered. Igracure 2959 has an activating frequency of 257 nm, but as UV light can lead to mutagenicity and phototoxicity, it is often used with a light source of 365 nm to minimize these toxic effects on the cells. This however leads to a lower reaction efficiency due to its low molar extinction coefficient (4 M^{-1} cm^{-1}) at this wavelength, meaning that the light exposure time or the Igracure 2959 concentration needs to be increased in order to compensate for this. LAP, on the other hand, has a molar extinction coefficient of 218 M^{-1} cm^{-1} at 365 nm, meaning that the reaction rate is much higher. LAP can also be used at 405 nm blue light, and even though the efficiency is lower compared to at 365 nm, using this wavelength of light would be beneficial for the cells [17]. The possibility of using LAP at both 365 nm and 405 nm at relatively low concentrations, and still achieving high crosslinking efficiency, makes it preferred over Igracure 2959 for this project.

In GelMA C, the advantages of GelMA with regards to bioactive components remain, but the printability is increased through the addition NFC [18]. The appearance of GelMA C is white and translucent, as opposed to pure GelMA which is clear and transparent [19]. The addition of xanthan gum and alginate in GelXA aims to increase the printability, ease-of-use and stability post-crosslinking. GelXA is also a white semi-translucent gel [20]. The appearance of the bioink can restrict the applications as a non-transparent bioink is more difficult to analyze in a microscope for e.g. evaluation of cell behaviour. However, the addition of these components giving the bioink increased printabiltiy and stability makes them beneficial for these purposes, which is why it is interesting to study and compare these bioinks.

2.4 Mesenchymal stem cells (MSC)

Mesenchymal stem cells (MSCs) are multipotent adult stem cells which can differentiate into osteoblasts (bone cells), chondrocytes (cartilage cells) and adipocytes (fat cells) [9]. Through several studies it has been confirmed that the mechanical properties of a hydrogel have an impact on the differentiation of MSCs [21], making them an interesting choice of cells to study. It has been shown that in a softer matrix, MSCs tend to differentiate into adipocytes and in a stiffer matrix they tend to differentiate to osteoblasts. The differentiation has however also been shown to depend on the hydrogel porosity, and the effect of the matrix stiffness independent of using osteogenic- and adipogenic-inducing medium is not yet concluded [21].

2.5 Rheological measurements

For measuring most complex, non-Newtonian flow behaviour, rotational or oscillatory tests on a rheometer can be used. A parallel plate measuring system, as illustrated in Figure 2.4, consists of two plates, of which the upper is attached to the rotor and constitutes the so-called measuring geometry. The lower plate is stationary and mounted onto the rheometer stand, sometimes referred to as the stage. The radius of the measuring geometry is defined as R, and the distance between the two plates is denoted H and is where the sample is placed [7].

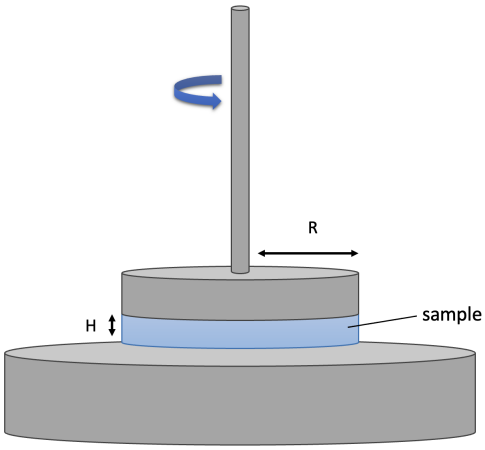

Figure 2.4: Schematic illustration of a parallel plate measuring system in a rheometer. R is the radius och the measuring geometry and H is the distance between the plates, which is where the sample is placed.

In rotational tests, the motor drives the moving plate into rotation by applying torque, either in the rotational or oscillatory mode. By controlling the torque and measuring the angular velocity and angular displacement of the sample, simultaneously recorded by an optical decoder, it is possible to convert this into stress, stain, strain rate, modulus and viscosity. Data analysis in the rheometer software interprets these rheological parameters to describe the properties of the sample [22]. It

is important to ensure that the measurements are performed within the linear viscoelastic region (LVE), where the viscoelastic parameters of the material are strain independent. The LVE occurs below a certain critical strain where the measurement does not effect or change the microstructure of the sample. The LVE is defined by the linear relationship between the complex stress and the oscillatory strain, but it can also be observed as a drop in storage modulus occurring at higher strain values when performing a sweep over a strain interval [23].

2.6 Cell analysis

To visualize cells and analyze their behaviour, fluorescence microscopy can be used. By staining different components of the cells with fluorescent dyes, the fluorescent molecules can be observed when illuminated at their absorbing wavelength. By viewing the emitted light through a filter that only allows this wavelength to pass through, the fluorescent molecules will glow against a dark background. Several dyes can be used simultaneously, but visualized separately in the microscope by switching between the different filters which are specific for each dye. This allows fluorescent staining of different cellular components which can later be combined and give information about the cells and their behaviour. [24]

2.6.1 Cell viability staining

Using Calcein-AM and propidium iodide (PI) allows for simultaneous live/dead staining of viable and dead cells. Calcein-AM is a highly lipophilic and cell membrane permeable chemical which can be converted into calcein by esterase in viable cells. The converted calcein emits a strong green fluorescence which will only be observed for viable cells. PI can stain the nuclei of a cell, but it cannot pass through cell membranes of viable cells. Therefore, only when penetrating a disordered membrane of a dead cell will PI reach the nucleus and intercalate the DNA, which then emits red fluorescence. Using a fluorescence microscope, simultaneous observation of the two dyes is possible, which can be used to calculate the percentage of viable cells [25]. Another dye that can be used in combination with Calcein-AM and PI is Hoechst, which is a blue fluorescent dye. It is cell permeable and stains nucleic acids in DNA, which means that it will stain all nuclei in a sample, both in living and dead cells [26].

2.6.2 Cell morphology staining

The cytoplasm of cells is spatially organized by a network of protein filaments known as the cytoskeleton, which in turn contains several different types of filaments that are responsible for different aspects of the cells spatial organization and mechanical properties. One type is the actin filaments that determine the shape of the cell's surface and that are also necessary for both migration and a part in the process for dividing one cell into two. The actin filaments are composed of subunits, called globular or G-actin, which assemble into a helix-shaped structure known as filamentous or F-actin [24]. To study cell morphology, staining of the F-actin in the

cytoskeleton together with the nuclei of the cells can be performed, to visualize their shape and structural organization. ActinGreen^{TM} 488 ReadyProbe (ThermoFisher Scientific) is a combination of the high-affinity F-actin probe phalloidin and a green fluorescent dye called Alexa Fluor 488. The high selectivity of phalloidin to F-actin in combination with the bright and photostable dye makes the F-actin visible in a fluorescence microscope [27]. For staining the nuclei, DAPI is commonly used as this fluorescent dye effectively binds to the DNA of cells. NucBlue^{TM} Fixed Cell Stain ReadyProbes^{TM} reagent (ThermoFisher Scientific) is a formulation of DAPI in a solution where it is stable at room temperature [28].

3
Methods

In this section the methods used for measuring the bioink samples' printability, viscoelastic properties and stiffness are described, followed by the methods used in the cell studies for cell culture, 3D bioprinting, and cell analysis.

3.1 Overview of experimental setup

The project can be divided into three main parts - printability, rheological measurements and cell studies, illustrated in Figure 3.1 as an overview of the workflow. The purpose of evaluating the printability was to investigate which printing conditions and settings were appropriate to use for the studied bioinks to achieve good printing fidelity. The rheological measurements were performed to investigate the viscoelastic properties of the bioinks when crosslinked using different methods and conditions. This was done by measuring the storage modulus of the bioink, which can be translated to the stiffness. For bioinks that are photo-crosslinked the crosslinking could be done in situ in the rheometer, allowing visualization of the increase in storage modulus as the crosslinking reaction is taking place. The bioinks which are crosslinked ionically or using dual crosslinking could not be crosslinked in situ in the rheometer, and instead had to be pre-crosslinked before the measurement. After some initial stiffness testing, two crosslinking conditions were chosen for each bioink to be evaluated further in stiffness measurements and cell studies.

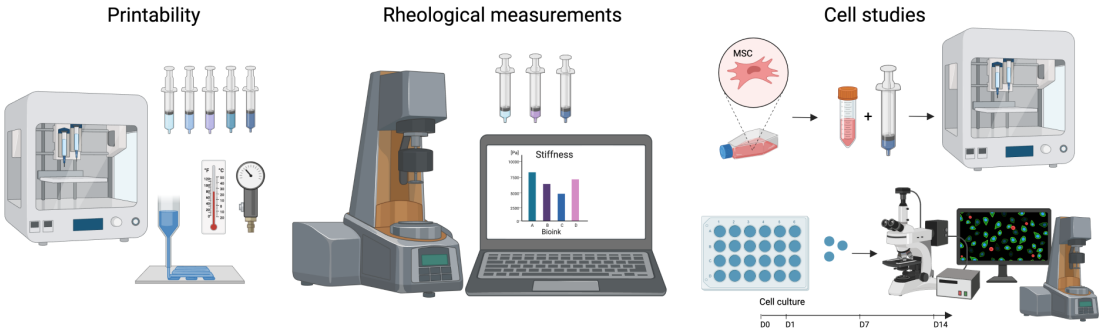

Figure 3.1: An overview of the three main parts of the project. Image created in BioRender.

For the cell studies 3D bioprinting was used to prepare samples of each bioink together with MSCs. The samples were printed in one full 24-well plate for each bioink and chosen crosslinking condition, cultured for 14 days and analyzed at day

0, day 1, day 7 and day 14. At day 0, stiffness measurements were performed only for the ionically crosslinked bioinks a few hours after printing. This was done to study any decrease in stiffness from day 0 to day 1. At day 1, three samples of each bioink and condition were used for analysis of the cell viability and the stiffness. These analyses were repeated at day 7 and day 14 according to the same procedure, and in addition three samples were fixated in paraformaldehyde (PFA) and saved for later analysis of the cell morphology.

3.2 Printability of the bioinks

To investigate the appropriate printing conditions of the temperature-dependent bioinks, a verification of the printing protocols for the GelMA-based bioinks was initially performed using a BIO X6 3D bioprinter. This was done by printing a more complex grid structure of dimensions 10x10x0.5 mm and investigating which pressure and potential pre- and post-flow delay settings would result in high printing fidelity at the bioinks' respective recommended printing temperature. Pre- and post flow delay is a setting that can be used to further control the pressure in the cartridge, and the resulting extrusion of bioink, as the nozzle is moving. Setting a pre-flow delay enables the extrusion to start before the nozzle starts moving, and can be used to avoid a gap occurring at the printed construct's starting position. In the same way, the post-flow delay can be used to control the extrusion at the last position of the print. The same test was also performed with a diluted version of each bioink, to simulate addition of cell suspension, with 10 parts bioink and 1 part HBSS (+/+).

3.3 Rheological measurements

For investigating the viscoelastic and mechanical properties of the bioinks, rheological measurements were made using a TA Instruments Discovery HR 10 rheometer with a parallel plate measuring system performing rotational and oscillatory tests. The three geometries used were a smooth upper peltier plate (UPP) 20 mm, a sand blasted 8 mm and a cross hatched 8 mm diameter. Before establishing these rheological methods, several measurement settings and strategies were tested and evaluated. This method development process is described in Appendix A. For each bioink, amplitude sweeps were performed to evaluate the LVE, to ensure the selected strain values were within that range.

3.3.1 Oscillation time sweep for in situ crosslinking

For the bioinks which are photo-crosslinked, the measurement of the crosslinked sample's stiffness was made using an oscillation time sweep and in situ crosslinking. This was done using a special setup in the rheometer consisting of a transparent glass stage as the bottom plate. The light source (405 nm) was placed directly underneath the sample at a 5 cm distance, which corresponds to the distance used for crosslinking in the BIO X printer. The bioink sample to be measured was first placed in a heating block at 37 °C for a minimum of 15 min, and then transferred

to the stage of the rheometer using a positive displacement pipette. The sample volume was between 160 and 180 µl for all samples. During this procedure, the UPP 20 mm geometry was already pre-heated to the printing temperature for the tested bioink. The measuring geometry was first lowered to the trimming gap at 550 µm, where any excess bioink was removed, and then lowered to the measuring gap of 500 µm as the measurement was started. In the measurement, the sample was equilibrated for 5 min at the printing temperature before switching to 21 °C, simulating the printing procedure in the BIO X printer. An oscillation time sweep was run for 5 min, at 0.5 Hz and either 1 % or 0.1 % strain, measuring the storage modulus of the sample. After 2 min, the light was switched on for the desired time span, which resulted in the sample being crosslinked.

3.3.2 Frequency sweep for pre-crosslinked samples

For the bioinks which are crosslinked ionically, or using dual crosslinking, the measurement of the crosslinked sample's stiffness was made using an oscillation frequency sweep on pre-crosslinked samples. To achieve the right sample size to fit the 8 mm geometry, a BIO X6 printer was used to print 8 mm diameter disks, with a height of around 500 µm. The disks were crosslinked, placed in HBSS (+/+) to prevent them from drying and measured shortly thereafter. The sample was carefully transferred to the rheometer using a spatula and placed in the centre of the 25 °C bottom plate. The geometry was lowered slowly until an axial force of either 0.1 N, 0.2 N or 0.5 N was observed, and then the run was started. The frequency sweep measured 0.1-10 Hz at either 1 % or 0.1 % strain, and the stiffness value, i.e., the storage modulus, at the measuring point of 0.5 Hz was used as the measured stiffness value. A frequency of 0.5 Hz was used both in the oscillation time sweep for in situ crosslinking and the frequency sweep for pre-crosslinked samples, as this had previously been confirmed to be a suitable frequency for generating stable data for samples in the same range.

3.4 Cell culture

For all cell experiments, immortalized MSCs were used. The cell line, ASC52telo, was purchased from ATCC and was originally isolated from the adipose tissue of a female donor in 2006. The cell line was immortalized using human telomerase reverse transcriptase (hTERT). The MSCs were cultured in T-flasks with high glucose Dulbecco's modified eagle medium (DMEM) with 10 % fetal bovine serum (FBS) and 1 % pest, and incubated in an incubator at 37 °C and 5 % CO_2. During cultivation the cell media was changed three times/week and once confluent, cells were passaged and re-seeded in new culture flasks.

When harvesting, the MSCs were prepared by removal of the cell media from the culture flask, followed by addition of phosphate buffered saline (PBS) for a few seconds. Trypsin was added for 5 min during incubation and the flask was then gently tapped on the sides in order to detach the cells from the surface. The trypsin was then neutralized by addition of cell media, which was also used to wash the flask and transfer the cells to a Falcon tube. The cells were centrifuged at 1000 rpm for 4

min. After removal of the supernatant, the cell pellet was resuspended in fresh cell media and the cells were counted to determine the cell concentration. Cell counting was done using a Countess^{TM} II Automated Cell Counter (ThermoFisher). Equal parts cell suspension and Trypan Blue were mixed in a tube and then 10 µl were transferred to each of the two chambers on the Countess^{TM} Cell Counter Chamber Slide. Four cell counts were performed, two one each side, and the average cell concentration and cell viability was calculated.

3.5 3D bioprinting

Before printing, a 8.0x0.5 mm model of the disk construct was created and transferred as a stl-file to the BIO X printer. The infill pattern of the disk was set to concentric with a perimeter and 43 % infill density. The BIO X printer was placed inside a sterile laminar air flow (LAF) bench during preparation of the material. The bioink to be used was heated in a bead bath at 37 °C for a minimum of 30 min.

The desired cell concentration used for printing was 2M cells/ml bioink. To obtain this number of cells in the desired volume of cell media, an additional centrifugation step was used. Ten parts bioink was mixed with one part cell suspension using two syringes connected with a Luer lock adaptor. The mixing was performed carefully to avoid introduction of air bubbles in the mixture and continued until visually homogeneous, after 15-20 mixing cycles. The mixture was transferred to an empty 3cc cartridge using a Luer lock adaptor and placed in the temperature controlled printhead set to the bioink's specific printing temperature and left for 10 min. A 22g nozzle was then attached to the cartridge before it was placed back in the temperature controlled printhead and connected to the air tube.

The nozzle was calibrated to the surface of a 24 well plate placed on the print bed, set to 15 °C, which had been measured to result in approximately 21 °C in the well plate due to poor thermal conduction through the plastic. The flow was tested, set to a suitable pressure and the bioprinting was started. One disk was printed in each well and once the whole plate was finished, photo-crosslinking was performed in the same order as the constructs had been printed, for the bionks where photo-crosslinking was used. The light module used had a wavelength of 405 nm and the distance to the samples was 5 cm. For samples to be crosslinked ionically, this was done following the photo-crosslinking. Ionic rosslinking solution was added to each well at a volume of 500 µl, either with concentration 50 mM $CaCl_2$ for 5 min or concentration 10 mM $CaCl_2$ for 2 h, before it was removed. To each well, 500 µl cell media was added and the well plate was then placed in the incubator at 37 °C and 5 % CO_2. The cell media was replaced with fresh cell media three times/week during the cultivation period.

3.6 Cell analysis

The cell behaviour in the constructs was evaluated on day 1, day 7 and day 14 of culture with different fluorescent staining assays. The stiffness of the constructs was also measured using the rheometer on the same days to monitor any change in stiffness over time. For each time point, 3 samples of each bioink and crosslinking condition was evaluated.

3.6.1 Cell viability staining

Cell viability staining was performed to investigate the viability of the cells in the constructs after printing. At each staining time, the samples to be evaluated were carefully transferred into a separate well plate using a spatula. Each well was prepared with 500 µl Hanks' balanced salt solution (HBSS) (+/+), in which the samples were initially incubated for 10 min.

The samples were stained with Calcein-AM at a concentration of 0.25 µg/ml in HBSS (+/+) during incubation for 30 min. Then, the Calcein-AM solution was removed and propidium iodide (PI) at a concentration of 100 µg/ml in HBSS (+/+) was added and incubated for 15 min. When evaluating samples later than day 1, a Hoechst staining at a concentration of 0.1 mg/ml in HBSS (+/+) was also added and incubated for 4-5 min. After removing the last staining solution, the samples were washed twice in HBSS (+/+), the first time for 5 min and the second time for 30-60 min. Before image analysis, a smaller volume of 150-200 µl fresh HBSS (+/+) was added to each well.

The samples were imaged directly in the well plate using an Echo Revolvee R4 microscope. Each disk was imaged in two positions, one at the edge of the disk and one in the centre at 4x magnification. A bright field image was taken to get an overview of the sample structure and then the fluorescent channels were switched to. The Calcein-AM dye was imaged in the Fluorescein isothiocyanate (FITC) filter, the PI dye in the Texas Red (TXRED) and the Hoechst dye in the 4',6-diamidino-2-phenylindole (DAPI) filter. The sample was first overviewed in the vertical plane to find a representative section and an overlay image of all channels was captured. Each channel was also saved in tiff-format for the analysis in ImageJ, where the number of live and dead cells was counted and used to calculate the cell viability.

3.6.2 Cell morphology staining

To later investigate the morphology of the samples, they were first fixated in PFA on day 7 and day 14. The PFA fixation aims to maintain the cells and their components in their current state and prevent any changes up until the point of further observation. To perform the fixation, the samples were carefully transferred to a separate well plate using a spatula, where each well was prepared with 500 µl HBSS (+/+). After 10-15 min, the HBSS (+/+) was removed, and approximately 300 µl 4 % PFA solution was added to each well. For ionically crosslinked samples, i.e.,

CELLINK and GelXA, the PFA was diluted in crosslinking solution, and for only photo-crosslinked samples PFA was diluted in PBS. The PFA solution was left for 5-6 hours to fixate the samples before it was removed. The samples were washed with HBSS (+/+) for 1-2 min, and then covered in fresh HBSS (+/+). The well plate was sealed with parafilm and placed in a fridge at 4 °C for storage until staining.

All fixated samples were collected and stained at the same time to be able to visualize the F-actin and the DNA of the cells in the constructs. The fixated samples were carefully transferred to a new well plate prepared with 500 µl HBSS (+/+) in each well. The three samples of the same condition were placed in the same well, adding up to a total of 20 wells. For staining of F-actin, ActinGreen™ 488 ReadyProbe (ThermoFisher Scientific) was used at a concentration of 1 drop/ml in HBSS (+/+). The HBSS (+/+) was removed after 15 min washing and 300 µl ActinGreen™ 488 solution was added to each well. The well plate was sealed with parafilm, covered in foil to protect if from light and left for incubation in room temperature overnight. The following day, the staining solution with NucBlue™ Fixed Cell Stain ReadyProbes™ reagent (ThermoFisher Scientific), a type of DAPI formulation, was prepared at a concentration of 2 drops NucBlue™/ml HBSS (+/+). The ActinGreen™ 488 solution was removed, replaced with 300 µl NucBlue™ in each well and incubated for 1 h in room temperature, covered in foil. The samples were washed with HBSS (+/+) three times for 10 min and then stored in HBSS (+/+) in a 4 °C fridge, protected from light, until analyzed in the fluorescence microscope.

The imaging took place at different time points in the following week after staining. Analysis of one condition at a certain time point was performed by transferring all three samples from that condition onto a glass slide, placed in the microscope. Some overview images were taken in the bright field channel, but the evaluation of the morphology was done using the fluorescent channels. ActinGreeen™ 488 was analyzed with the FITC filter and NucBlue™ with the DAPI filter. In 4x magnification, a few images were taken of each sample to visualize the general morphology and distribution of the cells. Using 20x magnification, individual cells and their morphology was analyzed by first scanning the sample and then capturing some representative images. Notes were also taken, describing the general perception of each sample and any other observations made.

4

Results and Discussion

The results from the different parts of the project are presented together with the discussion for each area. The results of the printability evaluation of the bioinks is presented first, followed by the different stiffness measurements performed. For the cell behaviour studies, the cell viability is presented first and then the cell morphology. The chapter is ended with a discussion on possible improvements and future research.

4.1 Printability of bioinks

The appropriate conditions for achieving good printability for the GelMA-based bioinks can be found in Table 4.1, displaying pressure and pre-flow delay at respective printing temperature.

Table 4.1: Appropriate conditions for achieving good printability for the GelMA-based bioinks. All diluted (dil.) bioinks were prepared with 10 parts bioink and 1 part HBSS (+/+).

Bioink	**Printing temp. °C**	**Pressure kPa**	**Pre-flow delay ms**
GelMA	25	17-27	0
GelMA (dil.)	25	20-30	0
GelMA C	24	25-35	-500
GelMA C (dil.)	24	20-30	-500
GelXA	24	27-37	-300
GelXA (dil.)	23	22-32	0

The post-flow delay was not used for any of the bioinks and it is therefore not included in the table. For GelMA Bioink, the recommended printing temperature from the printing protocol was actually 26 °C, but for this batch this seemed to be too high as the bioink was still runny after being equilibrated at 26 °C for over 30 min. The temperature was therefore lowered to 25 °C and the conditions for this temperature were evaluated. When printing with GelMA in the other experiments, 26 °C was tested first, and then the temperature was lowered if needed, depending on what seemed appropriate for the used batch.

4.2 Stiffness of crosslinked bioinks

The bioinks' stiffnesses were measured several times, first to initially investigate the stiffness range which could be achieved, functioning as a base when choosing which crosslinking conditions to continue investigating. After choosing two crosslinking conditions for each bioink, the stiffnesses at these conditions were tested again on the same bioink batches as used when printing together with cells, for the photo-crosslinkable bioinks using in situ crosslinking. This was done to generate data of the stiffnesses as similar to the stiffnesses being achieved in the 3D bioprinting process as possible. Lastly, the stiffnesses of the printed disks with MSCs were also measured throughout the experiment at day 0, day 1, day 7 and day 14 to investigate the stiffness with cells included.

4.2.1 Initial stiffness testing

During the initial stiffness testing some bioinks were also diluted to investigate which affect this had on the stiffness. An overview of all stiffnesses measured can be seen in Figure 4.1. The percentages in the graph refer to the amount of gelMA polymer in each bioink. As seen, GelMA and Photogel95 both contain 10 % gelMA polymer. The amount of gelMA written as X % cannot be specified due to confidentiality reasons, but it can be disclosed that the concentration X is lower than 10 % and the same concentration of gelMA polymer as in GelMA C and GelXA.

As observed in the graph, the stiffnesses achieved are in the order of between a few hundred Pa and roughly 10 kPa for all bioinks except Photogel95, which displays higher values. Comparing GelMA 10 % and GelMA X % (X $<$ 10 %), it is observed that the higher gelMA polymer concentration results in a higher stiffness. The addition of NFC to GelMA C and the addition of xanthan gum and alginate to GelXA results in a higher stiffness compared to GelMA X % for all three photo-crosslinking times. Both NFC and xanthan gum are materials which function to increase the viscosity or stability of a bioink, as previously described in the theory. By ionically crosslinking the alginate in GelXA after photo-crosslinking, an increase in stiffness is observed for 5 s photoX and 15 s photoX. The stiffness of GelXA crosslinked for 30 s and 5 min ionic (50 mM $CaCl_2$) not showing a higher value compared to the two shorter exposure times could be due to several reasons. Since all dual crosslinking GelXA stiffnesses were measured on bioprinted, pre-crosslinked samples, some variation in sample shape and evenness is possible. This could have lead to improper surface contact with the measuring geometry in the rheometer, resulting in a measured stiffness lower than the actual value. Another possible explanation is inhomogeneous material in the cartridge, where the bioink could have had a lower gelMA or LAP concentration in those two samples, which could lead to a lower stiffness being achieved.

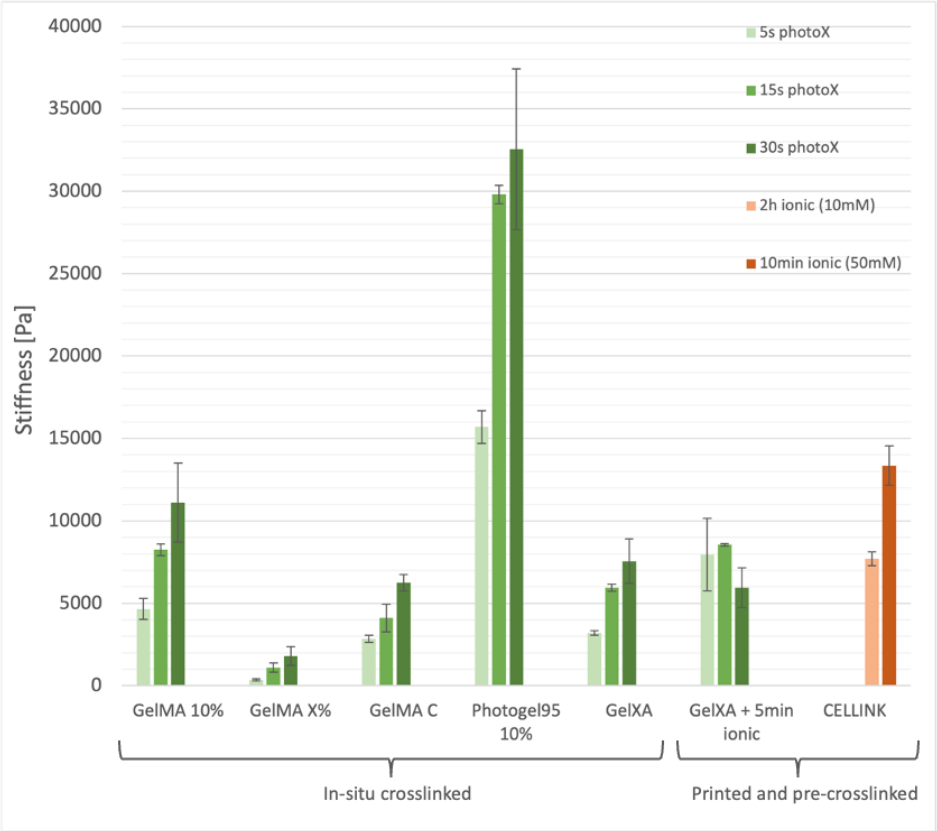

Figure 4.1: Overview of the initial stiffness testing, measured at 0.5 Hz and 1 % strain using either in-situ crosslinking in the rheometer or printing followed by stiffness measurement of pre-crosslinked samples, as marked in the graph. All photo-crosslinking was performed at 405 nm. The stiffness values are an average of two measurements and the error bars show the standard deviation. The percentages refer to the amount of gelMA polymer in the bioinks and the concentrations in mM refer to $CaCl_2$ in the ionic crosslinking solution.

It is obvious that the stiffness of Photogel95 is strikingly higher for all three photo-crosslinking conditions compared to the other bioinks. All three crosslinking times result in stiffnesses over 15 kPa, with the highest one at roughly 30 kPa. This shows the effect of the higher MA degree of 95 %, compared to GelMA with a MA degree of of 50 %. For all photo-crosslinked bioinks except GelXA (dual crosslinking), longer light exposure time leads to a higher stiffness. This demonstrates the principle that longer time for LAP to initiate the reaction between the MA groups leads to more chemical bonds and a more densely packed polymer network, resulting in higher stiffness. That the stiffness increases also at 30 s exposure time means that the amount of LAP, 0.25 % (w/v) in all used bioinks, is enough to keep the chemical reaction going and that the stiffness is not restricted to the amount of LAP.

Comparing the stiffnesses achieved with previous results in literature is desired, but due to the existence of many types of measurement methods for mechanical properties and the dependency of the results on the measuring set up, finding fully translatable results was difficult. In a study by Lee *et al.* [29], the stiffness of different gelMA-based bioinks was evaluated using a similar rheometer set up as in this project. The tests were performed on GelMA of 30 % polymer concentration with different degrees of MA, using 0.1 % Igracure 2959 as photo-initiator for UV light (wavelength not specified). The measurements were performed at 37°C, in the LVE, but at 1 Hz. The values of the storage modulus (stiffness) measured ranged from around 1000 Pa for 15 % MA to 10 kPa for 40 % MA and almost 100 kPa for 95 % MA [29]. These stiffness values are in the same order of magnitude as the ones measured for the gelMA-based bioinks in this project, although the measurement conditions, the gelMa polymer concentration and photo-initiator used differ.

In a study by Gonzalez-Fernandez *et al.* [11], the stiffness of different alginate-based hydrogels was investigated by 3D printing disks which were measured using a rheometer similar to the one used in this project. The disks were prepared without cells, crosslinked in 100 mM $CaCl_2$ for 5 min immediately after printing, submerged in growth media and evaluated at day 0 and day 7. The measurements were performed in the LVE at 1 Hz and 0.2 N axial force to obtain the storage modulus. For a hydrogel of alginate-NFC the stiffness at day 0 was 7.1 $\pm$ 0.6 kPa, which was maintained at day 7. Other alginate-based hydrogels decreased from day 0 to day 7, and had a lower stiffness also at day 0 compared to alginate-NFC (4.1 $\pm$ 0.6 kPa for a pure alginate hydrogel and 2.6 $\pm$ 1.1 kPa for an alginate-gelatin hydrogel) [11]. The stiffness of the alginate-NFC hydrogel is in the same range as what was measured for CELLINK Bioink, which ranges between almost 8 kPa and roughly 13 kPa.

The effect of the matrix stiffness on cell differentiation has been widely studied, and for MSCs the suitable stiffness range for investigating cellular mechanotransduction is around 0.5-50 kPa [30]. In a study by Engler *et al.* [31], the RNA expression of MSCs was studied for gels of different stiffnesses which showed that softer gels (elastic modulus 0.1-1 kPa) resulted in an upregulation of neurogenic expression, while moderately stiff gels (11 kPa) showed an upregulation of myogenic transcripts. On a stiffer gel of 34 kPa, the MSCs showed an upregulation in osteogenic expression [31]. The stiffnesses achieved in the initial stiffness testing (Figure 4.1), are within similar range of stiffness and could possibly be used in future studies of MSC differentiation.

Based on the results from the initial stiffness testing presented in Figure 4.1, two crosslinking conditions were chosen for each bioink. GelMA X % was not included in the continued experiments as it was primarily included as a way of evaluating the effect of the addition of NFC, xanthan gum and alginate. For GelXA, dual crosslinking was used in all continued experiments. The chosen crosslinking conditions are presented in Table 4.2.

Table 4.2: The two crosslinking conditions chosen to be used for each bioink in the continued experiments. The abbreviation "photoX" refers to photo-crosslinking at 405 nm.

Bioink	**Condition 1**	**Condition 2**
CELLINK	5min 50mM $CaCl_2$	2h 10mM $CaCl_2$
GelXA	5s photoX + 5min 50mM $CaCl_2$	15s photoX + 5min 50mM $CaCl_2$
GelMA	5s photoX	15s photoX
GelMA C	5s photoX	15s photoX
Photogel95	5s photoX	15s photoX

The photo-crosslinking times of 5 s and 15 s were chosen to be consistent and always using the same two crosslinking times, as this would make it easier to compare cell viability in-between bioink samples and conclude if a potentially low viability could be caused by the light exposure or other bioink-related factors. The longer crosslinking time of 30 s was avoided to decrease the potentially harmful effects on the cells.

The time used for ionic crosslinking with $CaCl_2$ was also lowered to 5 min instead of 10 min as in the initial measurements, for the same reason of not risking to harm the cells. Submerging 3D bioprinted constructs in ionic crosslinking solutions exposes the cells to a non-physiological environment which can damage the cells and lead to a lower viability in the constructs [32]. The calcium ion concentration in the cytosol of cells is in the order of 10^{-7} M [33], which is much lower than the concentration of $CaCl_2$ in the crosslinking solution, either being 10 mM or 50 mM. Therefore, a shorter ionic crosslinking time was chosen for the 50 mM concentration. The effect of using the lower concentration of 10 mM and a longer time of 2 h was tested as an alternative method, to investigate the effect this would have on the cells.

4.2.2 Stiffnesses at chosen crosslinking conditions

As there is sometimes variation between batches of bioink, another round of stiffness testing was performed with the chosen bioinks and respective crosslinking conditions for the same batches that were used in the cell experiments. The aim was to mimic the 3D bioprinting procedure as much as possible, using the in situ photo-crosslinking method, to be able to measure the same stiffness that the samples would have in the cell experiments. Therefore, these stiffness measurements do not include CELLINK Bioink which is ionically crosslinked and for GelXA, only photo-crosslinking was performed instead of dual crosslinking as in the cell experiments. Each crosslinking condition was measured in three repeats, with separate samples, and the average of the three measurements is presented in Figure 4.2 with a graph showing the whole measurement and the change in stiffness. Photogel95 is an exception where only two measurements could be made for each crosslinking condition due to low amount of sample available.

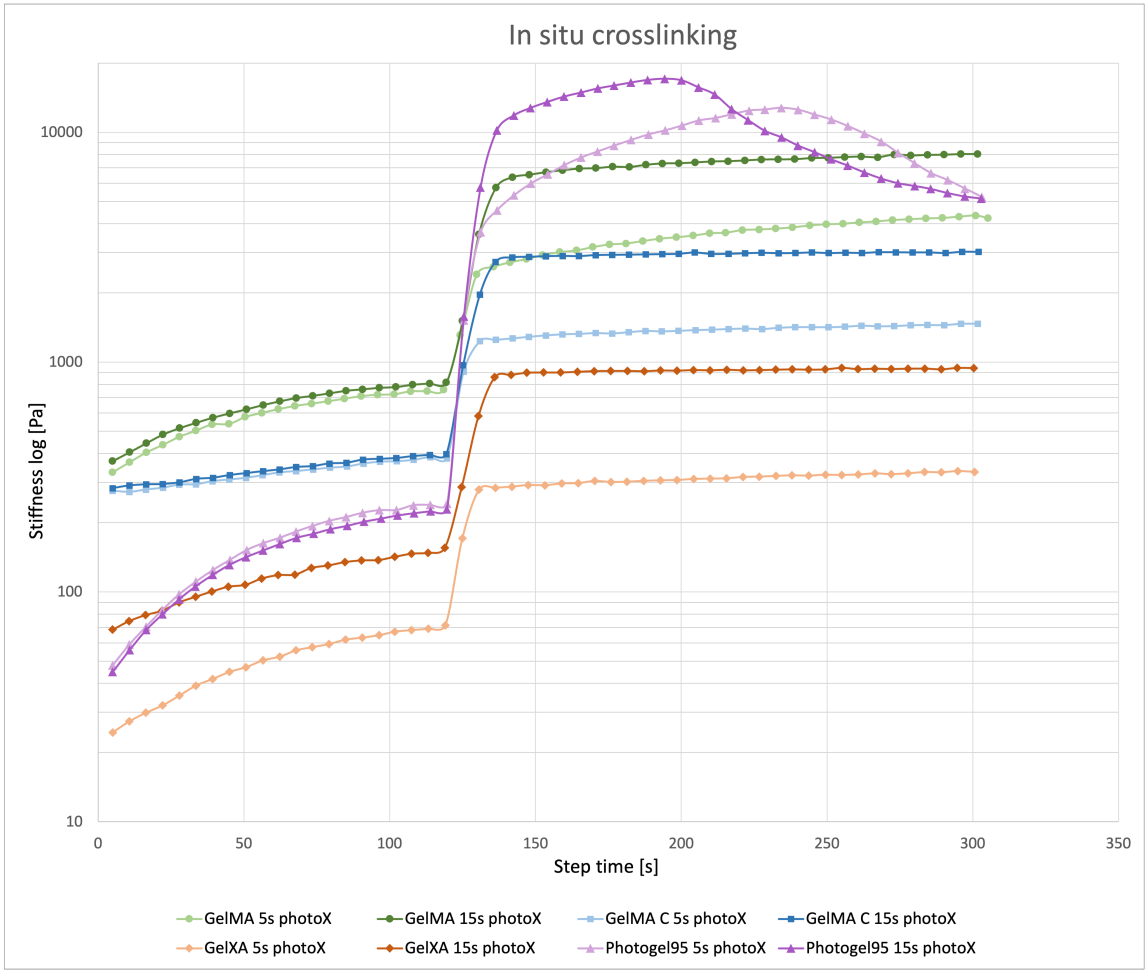

Figure 4.2: In situ crosslinking of the photo-crosslinkable bioinks. The data shown is an average of three separate runs, measured at 0.5 Hz and 0.1 % strain. Note that the y-axis is showing logarithmic values, and that the scale starts at 10 instead of 0 Pa.

In Figure 4.2, it can be observed that for all bioinks except GelXA, the stiffness value is roughly the same for each bioink at its non-crosslinked state in the beginning of the measurement, from 0 to 120 s. A slight increase is observed during this time interval, which can be explained by the polymer chains in the bioink undergoing some thermal crosslinking, even though the temperature is kept constant at 21 °C. Right before running the measurement displayed in the graph, each bioink has been equilibrated for 5 min at its printing temperature, so the increase in stiffness reveals that the process of cooling down from this temperature to 21 °C is still taking place. It also shows that thermal gelling is not an instantaneous process, which is why it is important to include equilibration time in the printing process.

That the non-crosslinked stiffness curves of the different conditions within each bioink are close to each other demonstrates that the thermal crosslinking process happens in a similar way every time. The difference between the different bioinks however, is a result of them containing different components at different concentrations, which is what contributes to the non-crosslinked viscoelastic characteristics of each bioink. For GelXA, showing a difference between the two conditions, an

explanation is that there probably was some variation and in-homogeneity in the bioink used for measuring the first condition compared to the second condition. Another interesting observation is that the stiffness of the non-crosslinked GelMA is higher compared to the non-crosslinked Photogel95, which both contain 10 % gelMA polymers, only with differing degree of MA. That the non-crosslinked stiffnesses are not the same, and that the one of GelMA is higher during the 2 min of equilibration at 21 °C indicates more thermal crosslinking, presumably due to a higher crossover temperature compared to Photogel95. Nevertheless, the final stiffnesses of the crosslinked Photogel95 are substantially higher compared to the final stiffnesses of both GelMA conditions.

Another observation of Figure 4.2 is that for all bioinks, the 15 s photo-crosslinking results in a higher final stiffness of the sample compared to the 5 s photo-crosslinking. The final stiffness value of each bioink and condition is also presented in Table 4.3, together with the standard deviation between the measurements. For all bioinks except Photogel95, the presented value is the average stiffness value of the last time point in the measurements. Since the stiffness of Photogel95 decreases after 200-225 s, the presented value in Table 4.3 is the average of the highest values reached during the measurements.

Table 4.3: The stiffness data from the in situ crosslinking measurements.

Bioink	**5s photoX Stiffness ± SD (Pa)**	**15s photoX Stiffness ± SD (Pa)**
GelMA	4 344 ±102	8 035 ±386
GelMA C	1 470 ±427	3 018 ±54
GelXA	333 ±60	942 ±144
Photogel95	13 154 ±1331	17 157 ±3

A similar decrease in stiffness of Photogel95 samples have been observed in previous measurements as well, and the reason behind it has been investigated. After each measurement of Photogel95, a small volume of condensed liquid has been observed on the glass stage when removing the sample. This has not been observed for any other bioinks. A possible explanation for this is that the quick contraction of the gelMa polymers resulting from the photo-crosslinking can cause the bioink to undergo what is known as syneresis. The process of syneresis is referring to when the network of a gel contracts and expels the pore liquid. Syneresis can be induced when increasing the concentration of polymer, leading to irreversible aggregation of the polymer chains in the gel network [34]. Since Photogel95 is so highly methacrylated (95 % MA), the gelMA polymers have many possible connection points that can bind to each other when exposed to the light during photo-crosslinking. The hypothesis is that when syneresis happens, at the peak in stiffness, the expelled liquid causes a slippage between the sample surface and the measuring geometry of the rheometer. This would impair the measurement and result in inaccurate values being generated. The occurrence of the assumed syneresis and the following decrease in stiffness makes it impossible to know if the highest stiffness measured at the peak is in fact the final stiffness of the sample, or if this value would in fact be even higher in reality. In the

in situ crosslinking measurements, the measuring gap is already set to automatically adapt to any changes in sample thickness by what is called active force control. It is evident that this setting cannot compensate for the assumed syneresis, and other attempts for adjustment of the measurement have unfortunately been unsuccessful in avoiding the observed stiffness decrease as well.

4.2.3 Stiffness of printed disks with MSCs

The results from the stiffness measurements of the printed disks with MSCs can be seen in Figure 4.3 and Figure 4.4. As previously described, the ionically crosslinked bioinks were measured at one additional time point at day 0 in order to study any early decrease in stiffness. At the other three time points, at day 1, day 7 and day 14, all bioinks were measured.

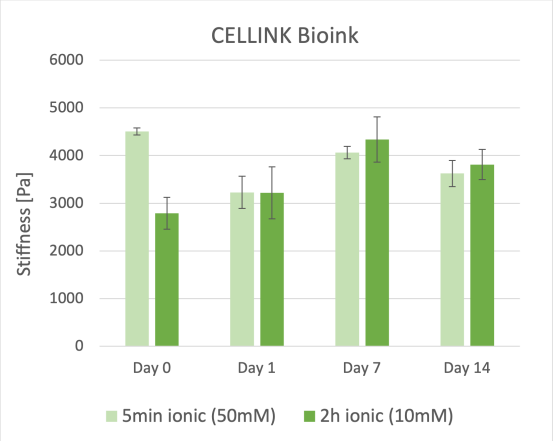

(a) Stiffness results for CELLINK Bioink.

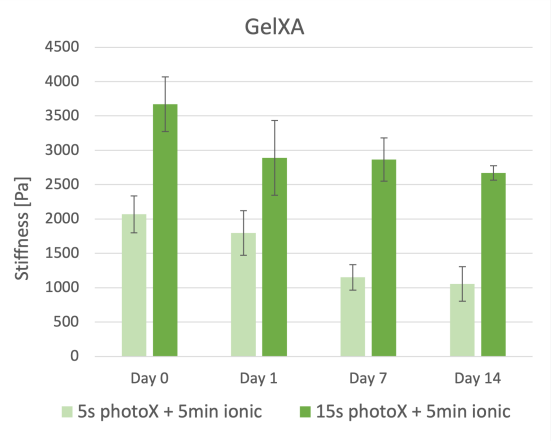

(b) Stiffness results for GelXA.

Figure 4.3: Stiffnesses of the printed disks with MSCs for CELLINK Bioink and GelXA, comparing the two crosslinking conditions. The bar shows the average stiffness of the three measured samples, along with error bars showing the standard deviation. The measurements were performed at 0.5 Hz and 0.1 % strain.

The results for CELLINK Bioink are presented in Figure 4.3a. It can be observed that the biggest difference between the two crosslinking conditions for CELLINK Bioink is at day 0, where 5 min of 50 mM $CaCl_2$ resulted in a higher stiffness compared to 2 h in 10 mM $CaCl_2$. For the other time points, the stiffness of the two crosslinking conditions is more similar but with some variation. Looking at the stiffness over time, it ranges between approximately 3 700 Pa and 4 500 Pa for all samples, which is relatively stable. From day 0 to day 1, a decrease of roughly 1 000 Pa is observed for the 5 min in 50 mM $CaCl_2$ condition, but instead an increase of a few hundred Pa is observed for the 2 h in 10 mM $CaCl_2$ condition. The variation between the measured samples, represented by the standard deviation in the diagram, is somewhat consistent throughout the different time points.

The stiffnesses of the GelXA disks, seen in Figure 4.3b, show a higher stiffness for the second crosslinking condition compared to the first one for all measured time points. For the first condition, the stiffness range is between roughly 1 000 and 2 000 Pa, and for the second condition the stiffness range is between roughly 2 500 and 3 500 Pa. Both conditions show a decrease in stiffness over time. This could be due to the ionic crosslinking not being stable over time since this is a type of physical crosslinking. A decrease in stiffness can result from the continuous dilution of Ca^{2+} ions in the sample, by depletion to the cell media. The photo-crosslinking, on the other hand, is chemical and should therefore be more stable.

The same trend with a continued decrease over time was however not observed for the CELLINK Bioink samples which are ionically crosslinked only. It is however possible that an immediate decrease in stiffness did occur before the rheological measurements were performed. The day 0 stiffness was measured approximately 4-5 hours after printing and crosslinking. Previous measurements of CELLINK Bioink, as presented in Figure 4.1, that were performed within minutes after the ionic crosslinking resulted in a stiffness at roughly 13 kPa for 10 min crosslinking (50 mM $CaCl_2$) and roughly 7 000 Pa for 2 h crosslinking (10 mM $CaCl_2$). These stiffnesses are both higher compared to the ones measured for the printed disks in Figure 4.3a. As the ionic crosslinking is depending on the concentration of Ca^{2+} ions in the sample, a long-term decrease in stiffness would be expected as the Ca^{2+} are depleted until equilibrium with the concentration in the cell culture media is reached. The cell culture media used, high glucose DMEM, contains several types of inorganic salts, including a concentration of around 1.8 mM $CaCl_2$. The potential more long-term decrease in stiffness for ionically crosslinked samples has not been investigated further.

The stiffness results for the photo-crosslinked bioinks can be seen in Figure 4.4. The stiffness of the GelMA disks varies throughout the experiment as seen in Figure 4.4a. At day 1, the second crosslinking condition shows a higher stiffness compared to the first condition, but at both day 7 and day 14 it is the opposite way around. The measured stiffness range of the first condition is roughly 2 000 Pa to approximately 4 500 Pa, while the second condition rages from almost 3 500 Pa at day 1 to around 2 000 Pa for day 7 and day 14. The standard deviation between the samples is very high, especially for the day 1 measurements. For GelMA C, seen in Figure 4.4b, an overall increase in stiffness is observed throughout the experiment. The stiffness of the first condition is approximately 2 000 Pa for day 1, 3 500 Pa for day 7, but returns to 2 000 Pa at day 14. The second condition increases from around 2 500 Pa at day 1 to 6 000 Pa at day 14. The standard deviation is relatively high throughout the measurements, and especially for the second condition at day 14.

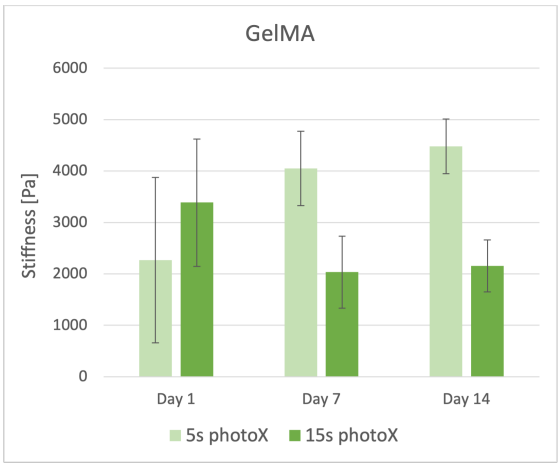

(a) Stiffness results for GelMA.

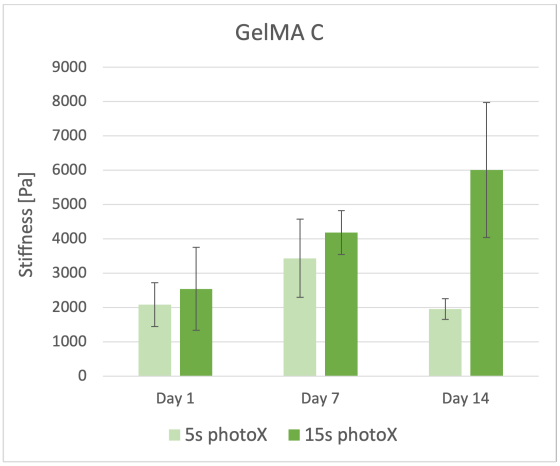

(b) Stiffness results for GelMA C.

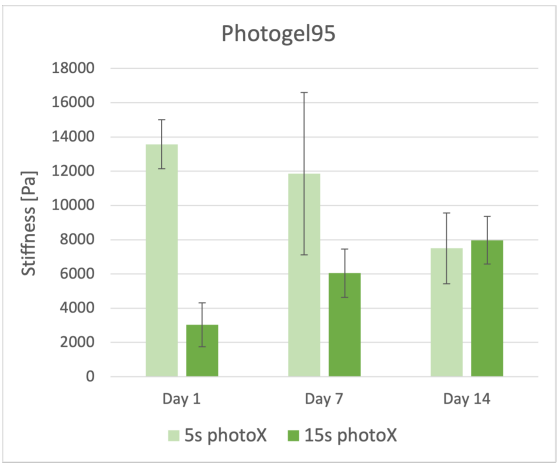

(c) Stiffness results for Photogel95.

Figure 4.4: Stiffnesses of the printed disks with MSCs for GelMA, GelMA C and Photogel95, comparing the two crosslinking conditions. The bar shows the average stiffness of the three measured samples, along with error bars showing the standard deviation. The measurements were performed at 0.5 Hz and 0.1 % strain.

The stiffness of Photogel95 is shown in Figure 4.4c. It can be observed that the measured stiffness values differ largely throughout the experiment. The first condition has a stiffness of over 13 kPa at day 1, around 12 kPa at day 7, but only roughly 7 kPa for day 14. The standard deviation is considerably higher for day 7, but also relatively high for the other time points. The stiffness of the second condition ranges from approximately 3 kPa at day 1 to 8 kPa at day 14, also showing a relatively large standard deviation between the samples. The perception of the samples' stiffness when handling them during the measurement was that the samples of the second condition were a least as stiff as the ones of the first condition. Compared to the perception of the other bioinks' stiffness, it was also experienced to be higher. The reliability of the stiffness results is therefore seen as very questionable for these samples.

A general observation of the stiffnesses of the printed disks with MSCs is that the results vary considerably both within the same crosslinking condition for different samples, and between the two crosslinking conditions of each bioink. The stiffnesses measured with in situ crosslinking, presented in Figure 4.2, show more reliable results with less variation between the three replicates and also a higher stiffness for samples that are photo-crosslinked at a longer time, which is theoretically reasonable. During the stiffness measurements of the disks with MSCs, several general observations and reflections were made, which are described below.

Firstly, some issues with the shape and size of the disks arised already in the 3D bioprinting step. As the printing process with cells included had to be performed in a sterile environment inside a LAF hood, and with the lights switched off to avoid unintentional crosslinking of the bioink during printing, difficulties in controlling and adapting the printing parameters were experienced. Disruptions in the bioink extrusion occasionally occurred due to low pressure or clogging of the nozzle. The thermal gelation leads to a higher bioink viscosity over time and subsequently requires adjustment of the pressure during the printing process, which at some points was unsuccessful. This sometimes resulted in uneven shape and surfaces of the disks. The step where the samples had to be transferred from the culture well plate for analysis at the different time points was also difficult for most of the bioinks. CELLINK Bioink was the only bioink where the samples had detached from the well plate, making it easy to scoop them up with a spatula. The other bioink samples had to be gently scraped off from the bottom of the well using the spatula, which was difficult to do without breaking them. The bioinks containing only gelMA polymers, i.e., GelMA and Photogel95, were especially hard to transfer since they were firmly attached to the well plate.

Since the rheological measurements are very sensitive and require proper contact with the sample's surface over the whole measuring geometry, uneven samples would disturb the measurements and the resulting stiffness value. Even though the method had been tested with other samples not containing cells, showing promising results without large variation between samples, this had not been done for stiffnesses covering the whole range. The guidance of the axial force value for when to start the measurement was also affected by the uneven sample surface, especially for the stiffer samples. In the case of a sample showing an uneven surface, the axial force could indicate that e.g., 0.1 N was achieved, when this was in fact only resulting from a part of the sample being in contact with the geometry. The misleading axial force value made it difficult to ensure proper surface contact for samples of varying shape and surface structure. Therefore, more testing and development of the method needs to be made to ensure correct measurements that generate more reliable stiffness results.

4.3 Cell behaviour

4.3.1 Cell viability

The viability of the MSCs in the printed disks is presented in the following section. In Figure 4.5, representative images obtained from the viability staining are shown. CELLINK Bioink crosslinked for 5 min in 50 mM $CaCl_2$ and GelMA photocrosslinked for 5 s are used as examples, showing day 1 and day 7 in both cases. The full viability data for all bioinks and crosslinking conditions, seen in Figure 4.6 and Figure 4.7, is based on the image analysis performed in ImageJ. Evaluation of viability was performed for all samples and conditions at day 1, day 7 and day 14 but due to the fluorescent staining being difficult to analyze for some bioink samples at day 14, this time point was decided to be excluded from the results for all bioinks. The image analysis was still performed but gave very high variation in viability between samples, making the results unreliable. Some viability data from day 14, as well as a more descriptions of the problems encountered can be found in Appendix B. By visual analysis of the images it was however observed that viable cells existed in all samples and crosslinking conditions at day 14.

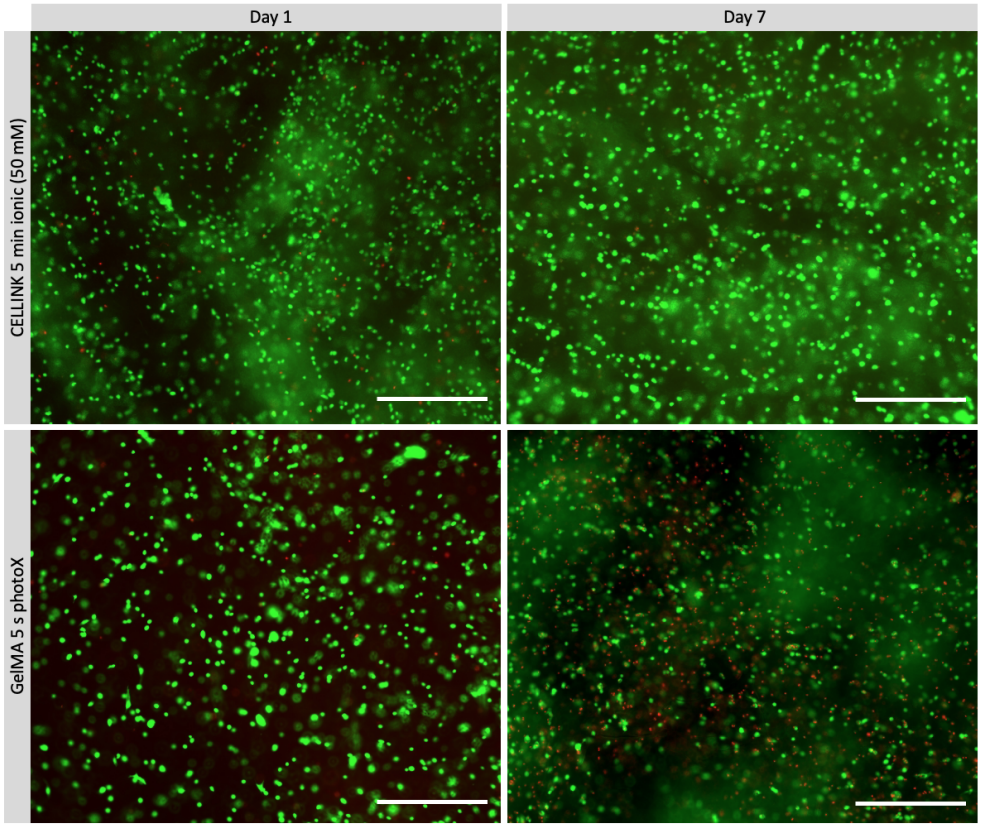

Figure 4.5: Two examples of images obtained from the viability staining, which were analyzed to calculate the cell viability. Live cells are visualized by the green fluorescence and dead cells by the red fluorescence. Scale bar showing 500 µm.

The viability data for each bioink is presented below, where the average viability of six images (from three separate samples) is shown together with the standard deviation in the error bars. A paired two-sample Student's t-test was performed to evaluate if the differences between day 1 and day 7 were significant for respective crosslinking condition. A significance level, α, of 0.05 was used and the conditions with a statistically significant difference are marked by the connecting line and the asterisk (*). In Figure 4.6a, the viability of the CELLINK Bioink samples can be found. The viability is high, above 90 % for both crosslinking conditions at both day 1 and day 7. The variation between samples, represented by the standard deviation, is relatively low. The high viability indicates that neither of the ionic crosslinking methods seem to have any considerable negative effects on the cells, short-term or long-term. The viability of the GelXA samples is presented in Figure 4.6b. At day 1, the viability of both crosslinking conditions is around 90 %, which is maintained to day 7 for the first condition but decreased to roughly 70 % for the second condition. The variation between the samples is higher compared to CELLINK Bioink, but relatively consistent within the different GelXA samples.

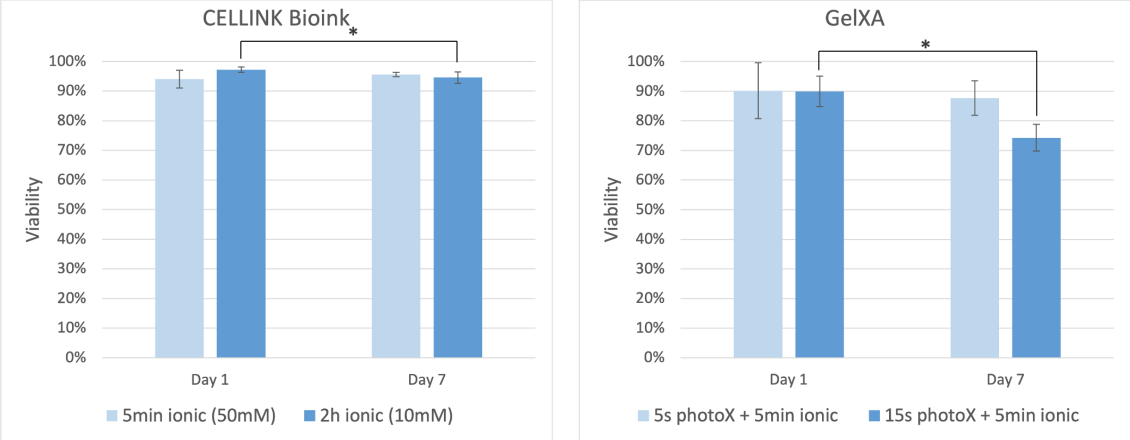

(a) Viability results for CELLINK Bioink. **(b)** Viability results for GelXA.

Figure 4.6: Viability of the cells for CELLINK Bioink and GelXA, comparing the two crosslinking conditions at day 1 and day 7. The bar shows the average viability of the three analyzed samples, along with error bars showing the standard deviation. Statistical significance: * $p < 0.05$.

The viability of the three photo-crosslinked bioinks, GelMA, GelMA C and Photogel95, is presented in Figure 4.7. The viability of the GelMA samples, seen in Figure 4.7a, shows high viability at day 1, above 85 % for both conditions. At day 7 a decrease is observed, primarily for the first condition of 5 s photoX which has a viability of roughly 50 %. The standard deviation between the samples is higher at day 7 than at day 1 for both conditions. The GelMA C samples show similar viability results, as seen in Figure 4.7b. At day 1, it is around 80-90 %, followed by a decrease at day 7. In this case it is however the second condition, 15 s photoX, that shows the lowest viability of around 50 %, while the first condition is around 65 %. The standard deviation between the analyzed samples also increases substantially from day 1 to day 7. For the Photogel95 samples, seen in Figure 4.4c, the viability is

very high at day 1, at around 95 % for both conditions. A big decrease is observed for day 7, where both conditions show approximately 55 % viability. As for the other bioinks, the standard deviation is higher at day 7 compared to day 1.

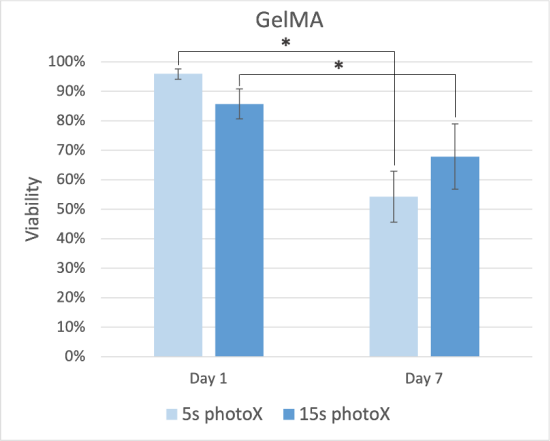

(a) Viability results for GelMA.

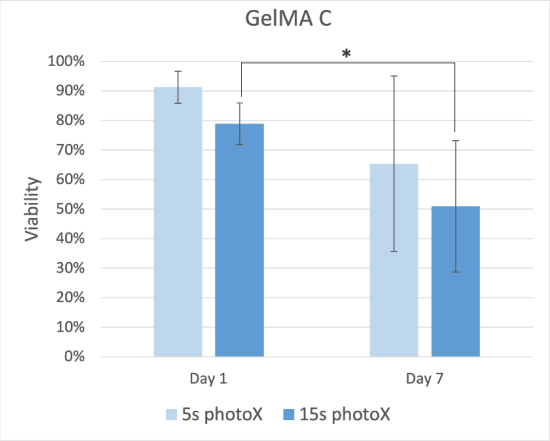

(b) Viability results for GelMA C.

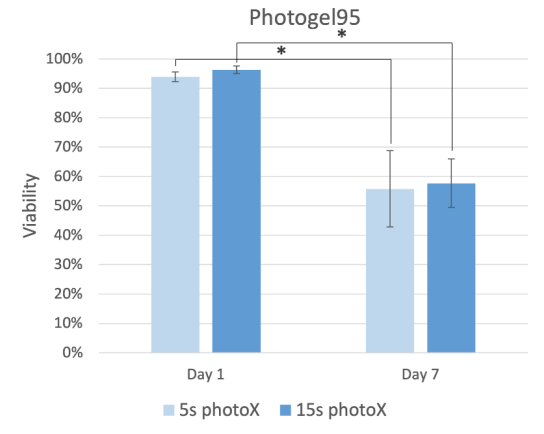

(c) Viability results for Photogel95.

Figure 4.7: Viability of the cells for GelMA, GelMA C and Photogel95, comparing the two crosslinking conditions at day 1 and day 7. The bar shows the average viability of the three analyzed samples, along with error bars showing the standard deviation. Statistical significance: * $p < 0.05$.

The high viability observed at day 1 for all bioinks and crosslinking conditions confirms that most cells survived during the printing process. A critical step that could cause the cell membranes to break is the extrusion thorough the nozzle where shear stress occurs. A ruptured cell membrane would cause immediate cell death that would have been observed already at day 1. The decrease in cell viability at day 7 can be caused by several factors. One possible reason is a more long-term effect of the photo-crosslinking as the exposure of the cells to light can introduce mutations in the DNA which could result in dysfunction of important cellular processes, leading to cell death. That the day 7 viability for GelXA and GelMA C is lower at the second crosslinking condition with a longer light-exposure time compared to the first condition, could be a sign of the harmful effects of the photo-crosslinking.

The relatively high standard deviation of the samples, primarily for GelMA C at day 7, and the fact that the same trend is not observed for the viability of GelMA and Photogel95 at day 7 prevents any conclusions from being made.

The cell viability can also be affected by the photo-crosslinking reaction itself. When exposing LAP, and other photo-initiators, to light, free radicals are generated which react with the monomers to form new covalent bonds and crosslink the polymeric material [17]. In the polymerization reaction, additional free radicals are formed as the already existing radicals react with the monomers, which keeps the reaction going. In a termination stage, the free radicals react with each other to terminate the polymerization reaction [17]. The free radicals forming during the crosslinking reaction could be harmful for the cells and decrease the cell viability. Investigating this effect on the cells and comparing different photo-initiators would be useful for future studies.

Other factors affecting the cell viability are the components of the bioink itself, as well as the stiffness and polymer network density achieved through the crosslinking. As mentioned in the theory section, cells prefer and thrive in more porous environments where they are not confined by a dense polymer network. The stiffness measurements of the printed disks with MSCs unfortunately showed high variation between samples and deviations from the stiffnesses observed for the different crosslinking conditions in the in situ crosslinking measurements. This is however believed to be related to issues with the sample preparation leading to errors and some inaccuracy of the results. It is therefore assumed that a longer photo-crosslinking time would lead to a more stiff bioink with more densely packed polymers, which is supported by both the theory of photo-crosslinking and the stiffness results presented in Figure 4.2 and Figure 4.1. According to the stiffnesses from the in situ crosslinking measurement, also presented in Table 4.3, the highest stiffnesses are achieved for GelMA and Photogel95. GelMA had a stiffness of roughly 4 000 Pa at 5 s photoX and 8 000 Pa at 15 s photoX, while Photogel95 had stiffnesses of roughly 13 kPa and 17 kPa at the respective conditions. For GelMA, the day 7 viability is at approximately 50-70 % and for Photogel95 it is around 55 %. This indicates a slightly lower viability for the stiffer samples. Since GelMA and Photogel95 both contain only gelMA polymers, the viability is not affected by any other biomaterial components, making it possible to do this comparison.

Lastly, looking at the method and cell viability analysis performed, there are some factors and procedure steps that should also be considered. Before the fluorescent staining could be done, the samples had to be transferred from the culture well plate to another staining well plate. This was done using a spatula and carefully trying to detach the disks from the well plate. As already mentioned related to the stiffness measurements of the printed disks, this was very difficult for some of the bioinks and at times resulted in small ruptures and damages of the disks. This handling and poking with the spatula may have mechanically damaged the cells, possibly causing disruption of the cell membranes, leading to cell death. It is believed that this potential immediate membrane damage would be possible to observe already in

the imaging, performed a few hours later.

The imaging and image analysis procedures rely partly on the judgment of the person performing them. Even though it was aimed to image all samples according to the same method, this can not be guaranteed and can have an effect on the final results. It is also difficult to be completely un-biased during the image analysis since some steps are qualitative and dependent on judgment and perception. However, since the viability analysis has been performed by the same person in all experiments, they are at least comparable to each other even though it can be difficult to compare them to results from other studies. The general increase in standard deviation from day 1 to day 7 can be related to the image analysis. By day 7, the cells have had time to potentially spread and proliferate, meaning that they can be more intertwined, making it hard to distinguish one cell from another. This had an even bigger effect on the day 14 samples, which were excluded from the data due to difficulties in the analysis, as previously mentioned.

4.3.2 Cell morphology

The results from the cell morphology staining are presented in the following section. The F-actin of the cells is visualized by the green fluorescence and the nuclei by the blue fluorescence. A general observation made during imaging was that at the samples' surface, a network of intertwined actin filaments was often seen, as shown in Figure 4.8a and Figure 4.8c.

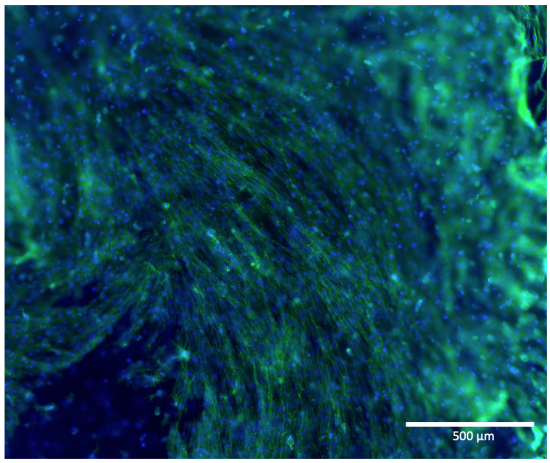

(a) Example of "2D-like spreading".

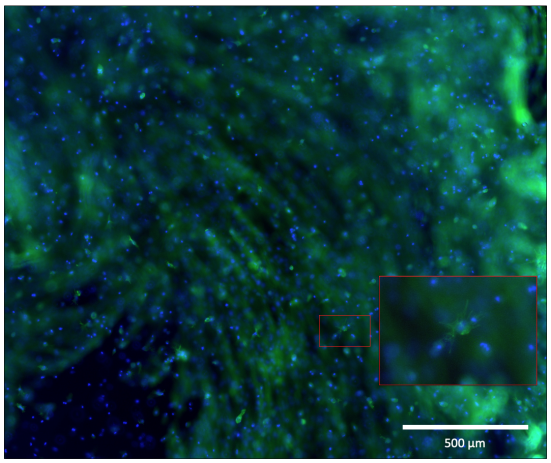

(b) Example of "3D-like spreading".

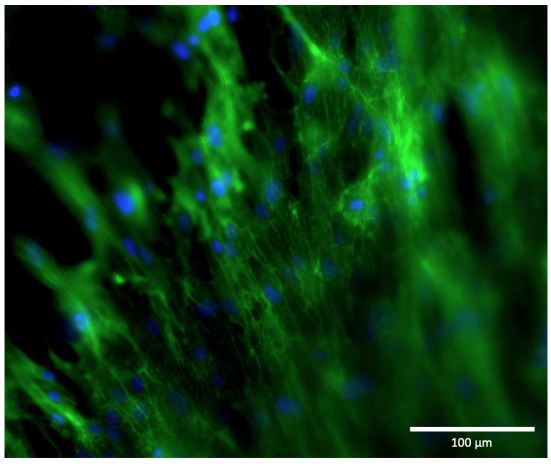

(c) Example of "2D-like spreading".

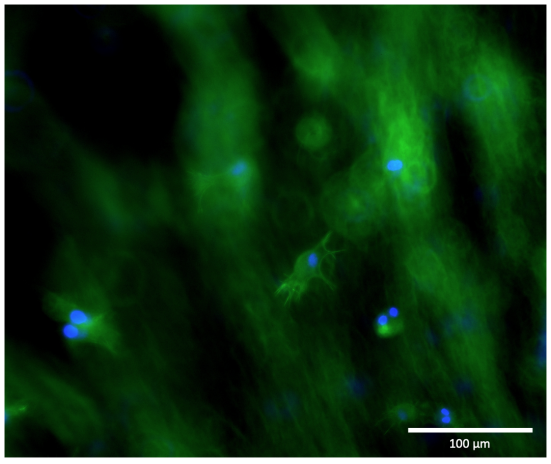

(d) Example of "3D-like spreading".

Figure 4.8: Images to show examples of the difference of what is described as "2D-like spreading" and "3D-like spreading" of the cells. All four are images of GelMA at day 7, crosslinked with 5s photoX, at different magnification. The images in (a) and (b) are showing exactly the same position of the sample, but with a change in focus to visualize the surface of the sample for (a) and the inside of the sample for image (b). Images (c) and (d) also show the exact same position in the same way, but with higher magnification.

This type of cell spreading and actin filament attachment would represent the cell behaviour in 2D, on a surface. Inside the 3D environment of the disk, individual cells were observed which showed another type of spreading, as seen in Figure 4.8b and Figure 4.8d. As the aim of the morphology staining was to investigate the cell behaviour inside the sample bulk, this was focused on in the imaging and is what

will be evaluated as the cell behaviour, as well as visualized in the images below. Each crosslinking condition and time point is visualized by only one image, chosen to be as representative of what was observed throughout the sample as possible. The sample surface was however also analyzed for all samples and the observations for each bioink are described.

The cell morphology results for CELLINK Bioink can be seen in Figure 4.9. Similar cell behaviour is observed for both crosslinking conditions and time points, with cells of round shape not showing any spreading away from the nuclei. A small actin filament is seen at the bottom of one cell at day 7 for the second crosslinking condition, but apart from that no other signs of spreading were found. The 2D-like spreading, as shown in Figure 4.8, was only observed in two of the three samples at day 14 for the crosslinking at 2 h in 10 mM $CaCl_2$ and none of the other samples.

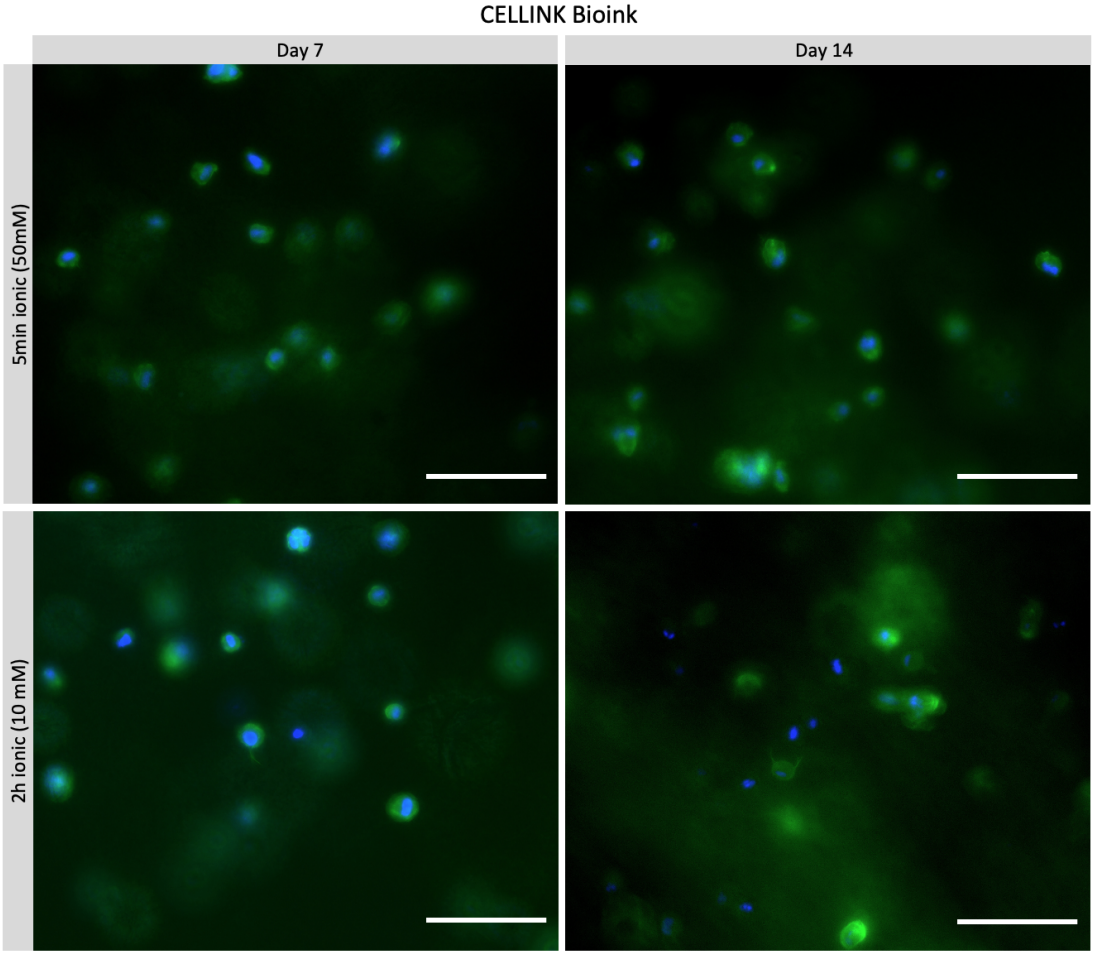

Figure 4.9: Cell morphology for CELLINK Bioink at the different crosslinking conditions and time points. The scale bar shown in each image is 100 µm.

The images showing the results of the cell morphology staining for GelXA are found in Figure 4.10. Here, cells with actin filaments spreading out from the nuclei are observed for both crosslinking conditions and time points. Several adjacent cells connecting to each other, forming small clusters, can also be seen. By seeing more than

one nuclei in close proximity, these can be distinguished from individual spreading cells. The observations made during the imaging, supported by the images chosen for Figure 4.10, lead to the perception that the different conditions and time points were similar with regards to frequency of spreading cells occurring. 2D-like spreading was observed on the samples' surface for both conditions at day 14, but at day 7 it was only observed for the first condition and not as much for the second condition. In the cases where this 2D-like spreading was observed it was more abundantly occurring at the sample edges, which makes sense since this part of the samples would have a larger relative surface area, compared to bulk volume.

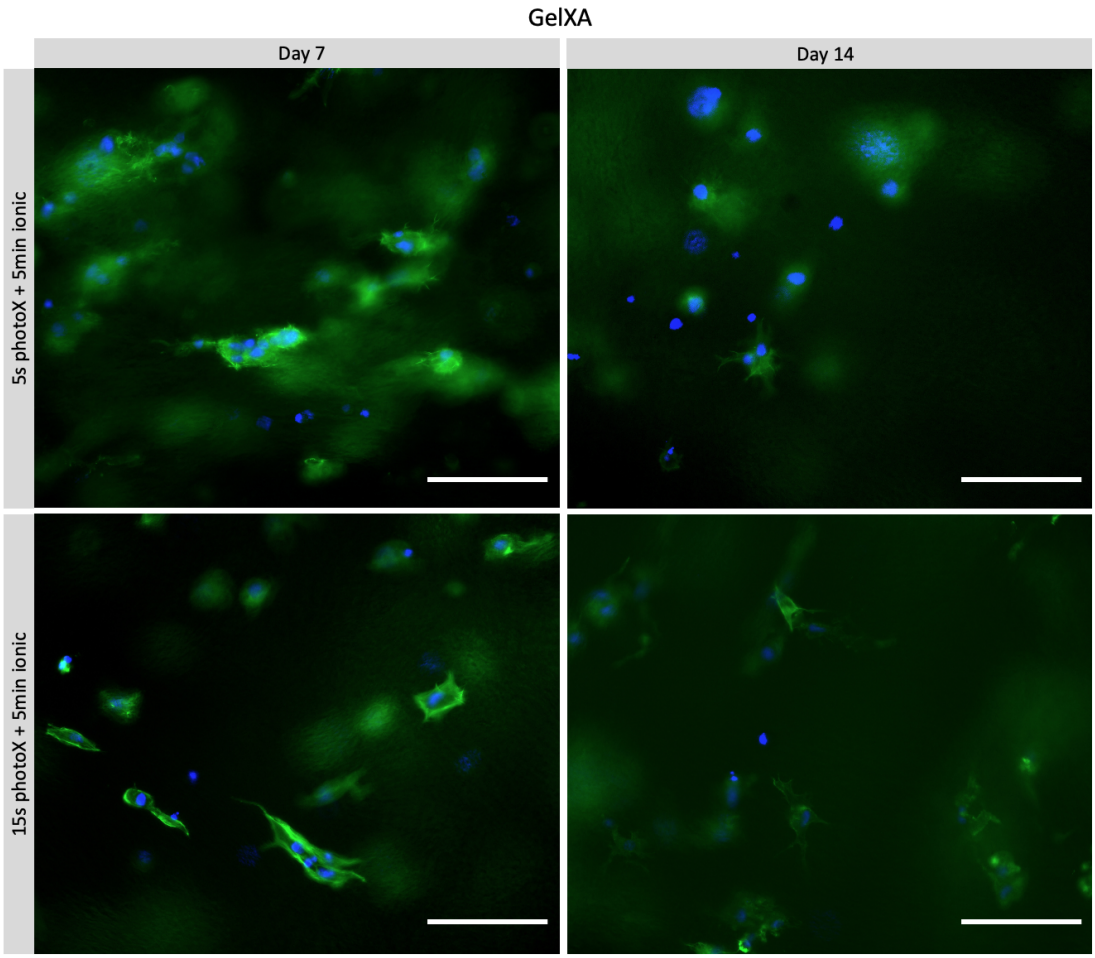

Figure 4.10: Cell morphology for GelXA at the different crosslinking conditions and time points. The scale bar shown in each image is 100 µm.

The cell morphology results for GelMA can be seen in Figure 4.11, where spreading cells can be seen for both crosslinking conditions and time points. From the chosen images, the second condition may appear to have a higher frequency of spreading cells as more are visible in the captured area. This can however be due to a higher cell density in those samples compared to the samples for the first condition, meaning that it should not be perceived as a higher degree of spreading. It can also be observed that there are several visible nuclei also in the first condition, at both time points, meaning that there are more cells present, without their actin filaments in

focus. The general perception during imaging was also that none of the conditions or time points were distinctively different throughout the whole samples compared to the others, leading to no conclusions about differences being possible to make. Occurrence of both 2D-like spreading on the surface and more 3D-like spreading inside the sample was observed in all samples for both conditions and time points of GelMA.

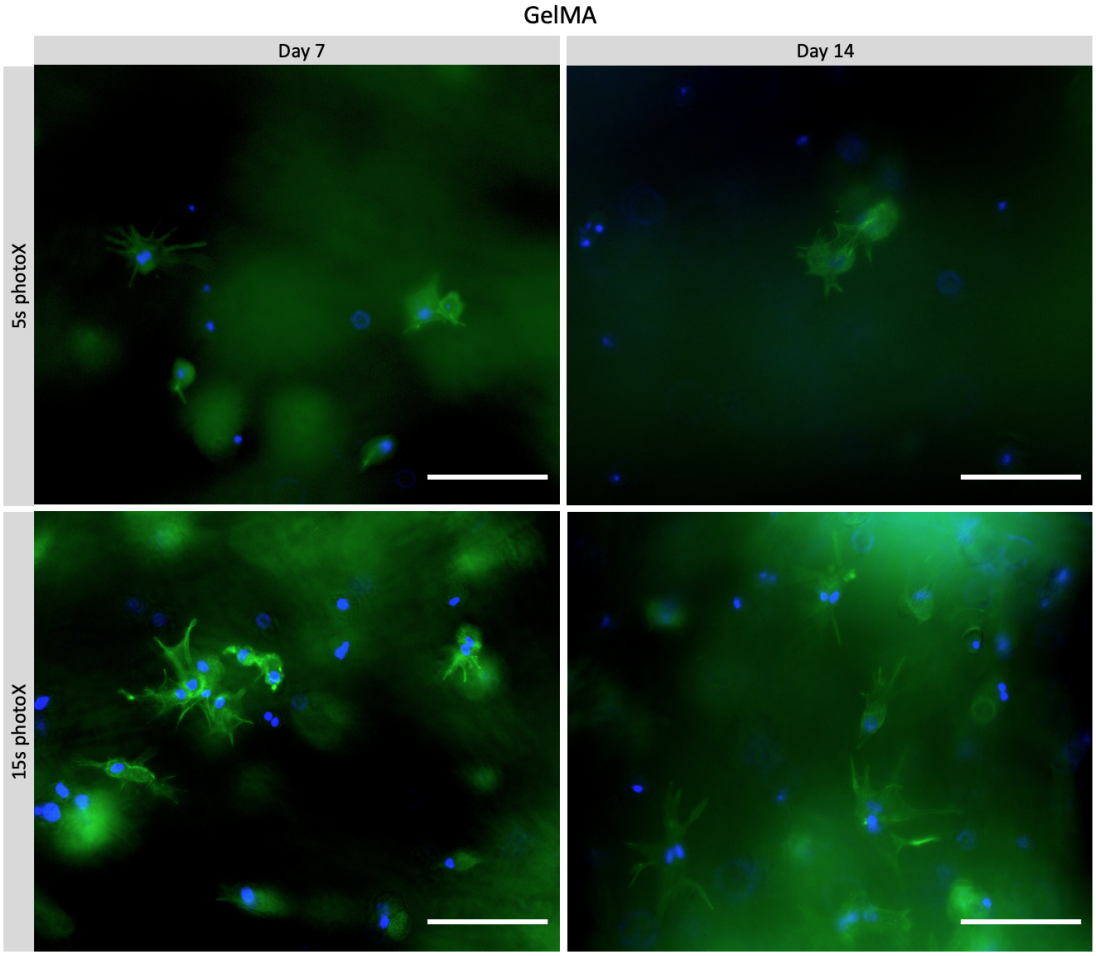

Figure 4.11: Cell morphology for GelMA at the different crosslinking conditions and time points. The scale bar shown in each image is 100 µm.

The cell morphology results for GelMA C are presented in Figure 4.12. As the images show, cells with spreading actin filaments are observed for both crosslinking conditions and time points, with no clear differences between them. Once again, the 2D-like type of spreading was observed at the sample surface and 3D-like spreading on the inside of the sample, for both conditions and time points.

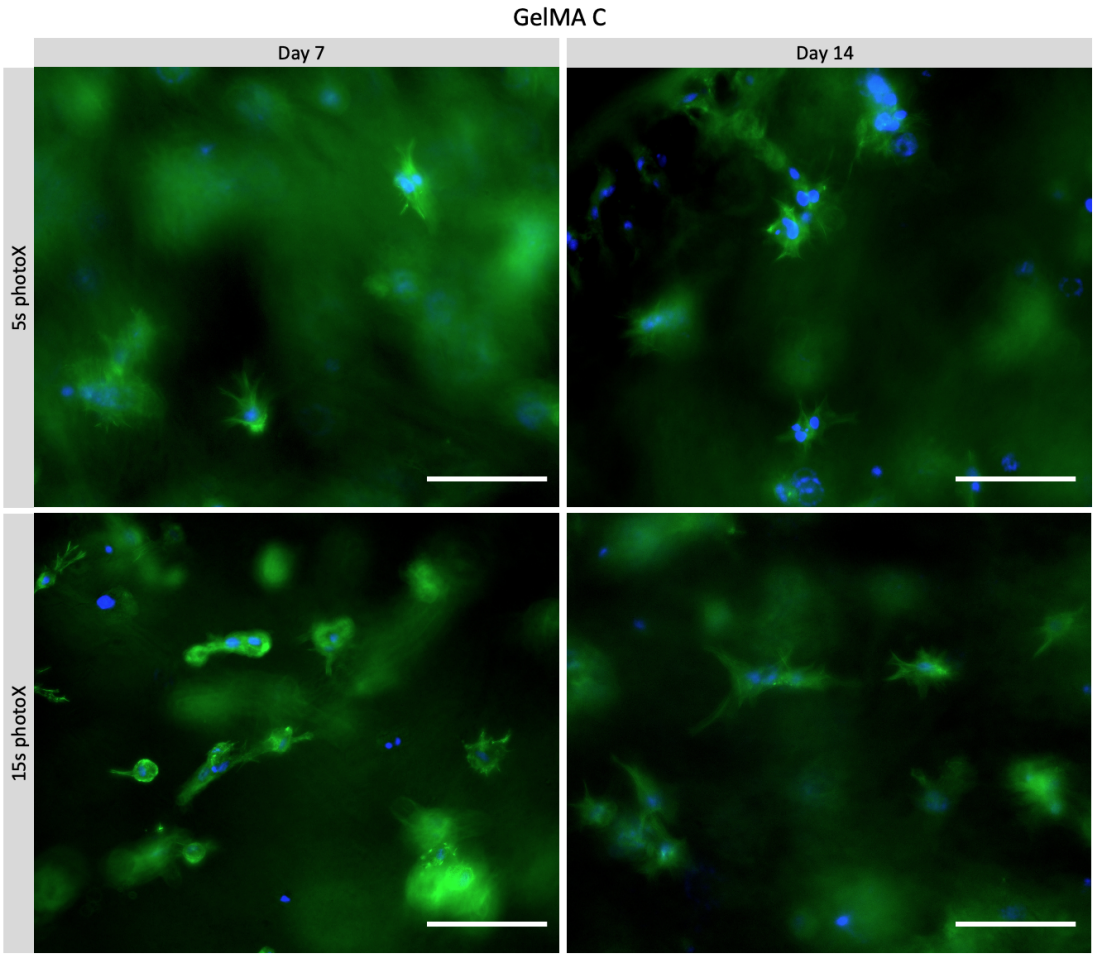

Figure 4.12: Cell morphology for GelMA C at the different crosslinking conditions and time points. The scale bar shown in each image is 100 µm.

The cell morphology results for Photogel95 can be seen in Figure 4.13. None of the crosslinking conditions at any of the time points show individual cells with spreading actin filaments in the bulk of the sample. The green fluorescence is surrounding the nuclei, showing a more round shape of the cells. At day 14 for the first condition, 5 s photoX, the cell in the centre of the image shows some attempt to spread its actin filaments out from the nuclei. The same thing was also observed for a small number of other cells in the other conditions and time points, not shown in the images in Figure 4.13. All of these were however only showing very short and few actin filaments spreading compared to the samples of GelXA, GelMA and GelMA C. Both conditions and time points were showing 2D-like spreading on the samples' surface where the cells were connecting to each other and forming some type of network, while the individual cells inside the sample had the morphology which

is shown in Figure 4.13. The lack of spreading actin filaments for the Photogel95 samples is likely due to the gelMA polymer network with 95 % MA being too dense and not porous enough for the cells to be able to spread. The ability of the cells to still create the 2D-like network on the surface of the samples shows that the cells can find attachment points and extend their actin filaments if they are not completely surrounded by the tight polymer network.

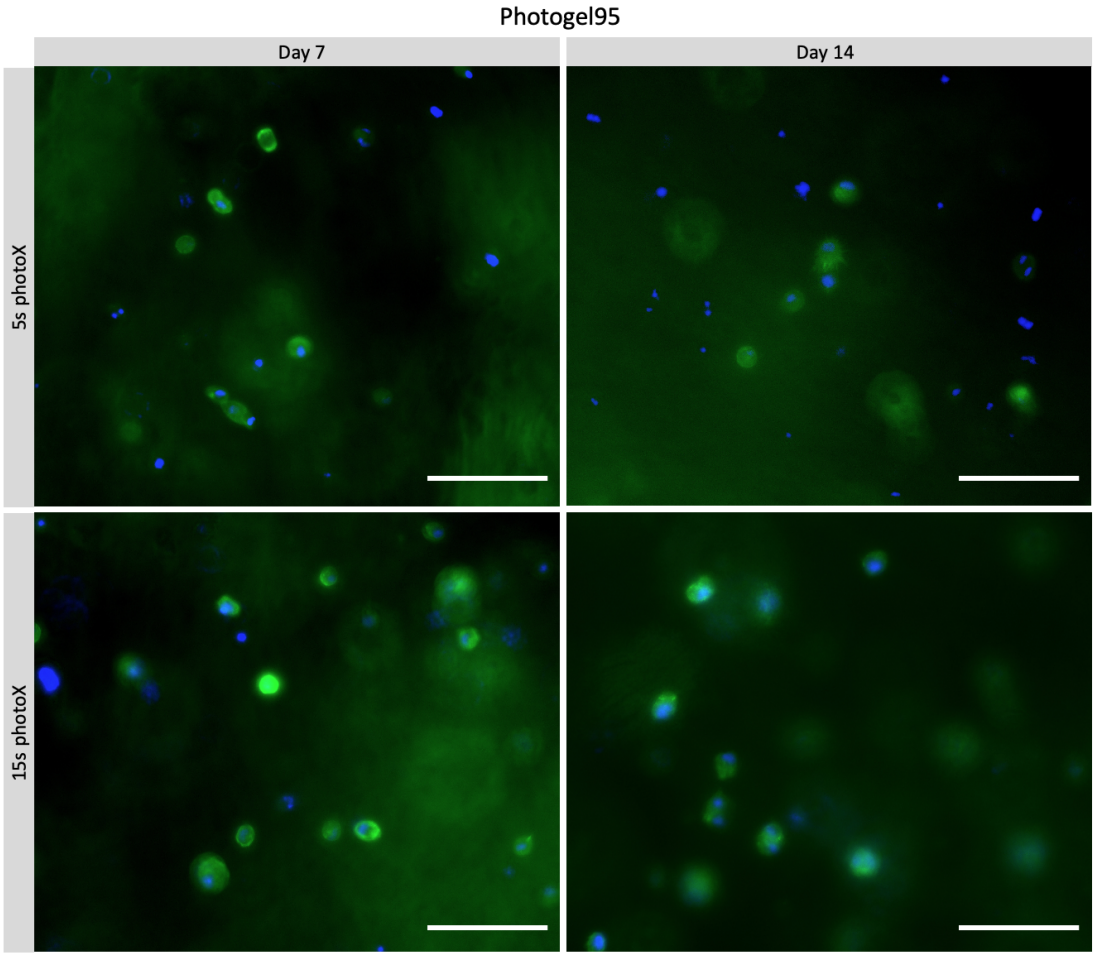

Figure 4.13: Cell morphology for Photogel95 at the different crosslinking conditions and time points. The scale bar shown in each image is 100 µm.

Combining the different results of the cell morphology, it can be concluded that the biomaterial components of the bioink influence the cell morphology. The cells in the CELLINK Bioink samples show no signs of spreading, which can be explained by the lack of biologically active components. Without structural and adhesive proteins in the cells extracellular environment, the cell surface receptors do not have anything to attach to. The gelMA-based bioinks, on the other hand, are composed of denatured collagen meaning that cell attachment points are naturally present. The cell morphology of Photogel95 differs from the other gelMA-base bioinks by not showing any spreading, or solely some small attempts of spreading. As previously mentioned, this is presumably related to the dense polymer network and high stiffness of the bioink making the cells unable to spread their actin filaments.

4.4 Improvements and future research

Based on the results and the method-related issues discussed, it is evident that some improvements and adaptation of the methods are possible. The rheological measurements of the printed disks with MSCs would improve if more uniform and smooth samples could be printed. This could be done by further optimizing the printing conditions for each bioink and performing more preparatory tests. Evaluating the axial force required to ensure proper surface contact with samples over a wider range of stiffnesses would also be useful. Another alternative could be to evaluate other methods for measuring the stiffness and mechanical properties of pre-crosslinked bioink samples. A suggestion is using nanoindentation, which was done in a study by Leu Alexa *et al.*, where gelMA-based hydrogels with different MA degrees and concentrations of photo-initiator were evaluated in terms of mechanical properties [15]. The indentation measurements are described to be performed in a rapid succession where the sample is automatically moved, enabling many indents to be made throughout the sample. The resulting measures of Young's modulus, which can be used to evaluate the compressive stiffness of a sample, displayed higher values for gelMA with a higher concentration of photo-initiator [15]. Nanoindentation was also used in another study by Jian *et al.*, where a 3D bioprinted model partly composed of gelMA-based hydrogel was evaluated to be used as a meniscal scaffold [35]. However, to generate accurate measurements using nanoindentation, the importance of the sample surface being even is emphasized. Therefore, the samples were set with epoxy resin and polished before the stiffness measurements, to ensure an even surface [35]. Before applying this method, it must however be verified that the epoxy resin treatment does not affect the measurements of the mechanical properties of the sample.

Regarding the evaluation of the cell behaviour, alternative methods to generate more quantitative data have been considered as a way of improving the analysis and providing results which are not as reliant on the perception of the person performing the analysis. For evaluating the cell viability, performing a PrestoBlue assay could be an alternative. PrestoBlue^{TM} Cell Viability Reagent (ThermoFisher) is a cell permeable resazurin-based solution which functions as an indicator of the metabolic reducing power of living cells. When resazurin is reduced, the solution becomes red and highly fluorescent, which can be observed by fluorescence or absorbance measurements. The change in intensity over time can be used to quantitatively measure the proliferation of the cells [36]. By using a plate reader to measure the intensity of the fluorescence or absorbance, many samples could be evaluated at the same time. Since a PrestoBlue assay would not depend on any visual image analysis, evaluation of cell viability of more long-term experiments should be possible, which would be an advantage for the day 14 analysis.

To allow comparison of cell morphology between different samples and conditions, quantification of the cell morphology would be required. Different strategies for quantification of cell morphology using image analysis and emerging programming tools like deep learning have been developed as a way of relating the cell morphol-

ogy to different states of the cell, to be used for e.g., prediction of formation of cancer tumours [37]. The development of a toolbox for quantifying cell morphology in MATLAB (Mathworks), called TISMoprh, is presented in a study by Alizadeh *et al.* [38]. In the study, PFA-fixated osteosarcoma cancer cells were stained for their nuclei and F-actin using similar fluorescent dyes as in this project. A very simplified description of the workflow is that the images from the fluorescent microscope were transformed using a set of tools, quantified according to its features and then analyzed using Principal Component Analysis (PCA) [38]. To be able to evaluate differences in cell morphology between different crosslinking conditions and bioink stiffnesses, using a method similar to this would be an interesting alternative.

For future investigation, the inclusion of more technical replicates as well as addition of biological replicates would be desired. This is a requirement for achieving higher reliability in the data and enabling conclusions to be drawn. To extend the research, it would also be interesting to investigate the effect on the cell behaviour if adding biologically active components, such as laminin and RGD, to CELLINK Bioink. In continuing to evaluate the influence of bioink stiffness on the cell behaviour, a possibility would be to investigate its effect on differentiation of MSCs to different cell types. It could also be investigated if a combination of stiffness and growth factors could make the differentiation of MSCs more efficient compared to using growth factors solely.

5
Conclusion

After investigation of the viscoelastic properties of the bioinks, some conclusions can be made. Firstly, is has been shown that batch variations affect the printability of the bioink and which printing conditions that are appropriate for achieving high printing fidelity. The stiffness of the bioinks after crosslinking are also affected by variations in the material, which can be both due to batch variations and other factors like inhomogeneity in the sample due to insufficient mixing. Comparing the different methods used for measuring the stiffnesses of the crosslinked bioinks, the in situ crosslinking shows relatively high repeatability and reasonable results while the measurements of pre-crosslinked samples show higher variation, especially for the printed disks with MSCs. The range of stiffness which was achieved for the evaluated bioinks was between a few hundred Pa and roughly 30 kPa in the initial stiffness testing. The highest stiffnesses were measured for Photogel95.

The stiffnesses achieved at the two selected crosslinking conditions, also used in the cell experiments, were between roughly 300 Pa and 17 kPa according to the repeated in situ crosslinking measurement for the photo-crosslinkable bioinks, made on the same batches as used when printing. As the stiffness measurements of the printed disks with MSCs were not really in line with these previous stiffnesses measured, and due to the high variation between the samples, these were seen as unreliable and could not be used as a base for any conclusions. To successfully measure the stiffness of samples with cells included, the method needs to be optimized and adapted further, or other options could be investigated.

The cell viability results showed a high viability at day 1 for all bioinks and crosslinking conditions, above 90 % for most samples but around 80 % for a few. At day 7, the viability of both CELLINK Bioink conditions was still high, while all the other bioinks which had been photo-crosslinked had decreased in viability. This could be a sign of the light-exposure during crosslinking resulting in more long-term harmful effects for the cells, which cannot be observed until at day 7. For both GelXA and GelMA C, the second condition with 15 s photoX resulted in lower cell viability compared to the first one, but for GelMA and Photogel95 it was the opposite way around or a lower viability for the first condition. That a longer photo-crosslinking time of 15 s is more harmful for the cells compared to 5 s photo-crosslinking could therefore not be verified and no conclusions regarding the influence of the crosslinking conditions on the cell viability could be made. Comparing the crosslinking methods suggests that the ionic crosslinking might be less harmful for the cells compared to the photo-crosslinking in a more long-term perspective. However, it needs to be

considered that the different crosslinking methods are used on completely different bioinks, which also has an effect on the cell viability, making it impossible to draw any definite conclusions.

The results of the cell morphology analysis showed many cells with spreading actin filaments in both crosslinking conditions for GelXA, GelMA and GelMA C. A difference in the amount of cell spreading observed could however not be concluded when comparing the two crosslinking conditions for any of the bioinks. Some attempts of spreading were observed for a small number of cells in both Photogel95 conditions, but overall the cells were defined as non-spreading in the bulk of the sample. In CELLINK Bioink, no spreading cells were observed in any of the crosslinking conditions. The spreading observed in the gelMA-based bioinks demonstrates the importance of the cells having biologically active components in their environment to be able to attach to something. That the cells did not spread in the Photogel95 samples, which are also gelMA-based, implies that the polymer network is too dense and stiff to allow any cell spreading to take place. The reason for the cells not spreading in the CELLINK Bioink samples is likely due to the lack of biologically active components.

The different methods that were developed and used to measure the stiffness of the bioinks, to study the effects on the cell behaviour, require continued development to be able to make any definite conclusions. The results from this project however form a base for this development and provide meaningful knowledge which can be investigated further.

Bibliography

[1] Directorate-General for Environment. *Animals used for scientific purposes*. URL: https://ec.europa.eu/environment/chemicals/lab_animals/3r/alternative_en.htm.

[2] Vijay K Singh and Thomas M Seed. "How necessary are animal models for modern drug discovery?" In: *Expert Opinion on Drug Discovery* 16.12 (Dec. 2021), pp. 1391–1397. ISSN: 1746-0441. DOI: 10.1080/17460441.2021.1972255.

[3] The Division of Transplantation (DoT). *Organ Donation Statistics*. Mar. 2022. URL: https://www.organdonor.gov/learn/organ-donation-statistics.

[4] Waeljumah Aljohani et al. "Bioprinting and its applications in tissue engineering and regenerative medicine". In: *International Journal of Biological Macromolecules* 107 (Feb. 2018), pp. 261–275. ISSN: 01418130. DOI: 10.1016/j.ijbiomac.2017.08.171.

[5] Jos Malda et al. "25th Anniversary Article: Engineering Hydrogels for Biofabrication". In: *Advanced Materials* 25.36 (Sept. 2013), pp. 5011–5028. ISSN: 09359648. DOI: 10.1002/adma.201302042.

[6] Yu Shrike Zhang and Ali Khademhosseini. "Advances in engineering hydrogels". In: *Science* 356.6337 (May 2017). ISSN: 0036-8075. DOI: 10.1126/science.aaf3627.

[7] Thomas G Mezger. *The Rheology Handbook*. 4th ed. Hanover: Vincentz Network, 2014. ISBN: 3-86630-842-6.

[8] Bingcheng Yi, Qi Xu, and Wei Liu. "An overview of substrate stiffness guided cellular response and its applications in tissue regeneration". In: *Bioactive Materials* 15 (Sept. 2022), pp. 82–102. ISSN: 2452199X. DOI: 10.1016/j.bioactmat.2021.12.005.

[9] Clemens A van Blitterswijk and Jan de Boer. *Tissue Engineering*. Ed. by J D Debruijn et al. 2nd ed. San Diego: Elsevier Science & Technology, 2014, pp. 48–54.

[10] Carmen C. Piras and David K. Smith. "Multicomponent polysaccharide alginate-based bioinks". In: *Journal of Materials Chemistry B* 8.36 (2020), pp. 8171–8188. ISSN: 2050-750X. DOI: 10.1039/D0TB01005G.

[11] Tomas Gonzalez-Fernandez et al. "Alginate-Based Bioinks for 3D Bioprinting and Fabrication of Anatomically Accurate Bone Grafts". In: *Tissue Engineering Part A* 27.17-18 (Sept. 2021), pp. 1168–1181. ISSN: 1937-3341. DOI: 10.1089/ten.tea.2020.0305.

[12] Kuen Yong Lee and David J. Mooney. "Alginate: Properties and biomedical applications". In: *Progress in Polymer Science* 37.1 (Jan. 2012), pp. 106–126. ISSN: 00796700. DOI: 10.1016/j.progpolymsci.2011.06.003.

[13] Xiaoju Wang, Qingbo Wang, and Chunlin Xu. "Nanocellulose-Based Inks for 3D Bioprinting: Key Aspects in Research Development and Challenging Perspectives in Applications—A Mini Review". In: *Bioengineering* 7.2 (Apr. 2020), p. 40. ISSN: 2306-5354. DOI: 10.3390/bioengineering7020040.

[14] Hossein Baniasadi et al. "High-resolution 3D printing of xanthan gum/nanocellulose bio-inks". In: *International Journal of Biological Macromolecules* 209 (June 2022), pp. 2020–2031. ISSN: 01418130. DOI: 10.1016/j.ijbiomac.2022.04.183.

[15] Rebeca Leu Alexa et al. "3D-Printed Gelatin Methacryloyl-Based Scaffolds with Potential Application in Tissue Engineering". In: *Polymers* 13.5 (Feb. 2021), p. 727. ISSN: 2073-4360. DOI: 10.3390/polym13050727.

[16] Heqi Xu et al. "Effects of Irgacure 2959 and lithium phenyl-2,4,6-trimethylbenzoylphosphinate on cell viability, physical properties, and microstructure in 3D bioprinting of vascular-like constructs". In: *Biomedical Materials* 15.5 (Aug. 2020), p. 055021. ISSN: 1748-605X. DOI: 10.1088/1748-605X/ab954e.

[17] Kamil Elkhoury, Julio Zuazola, and Sanjairaj Vijayavenkataraman. "Bioprinting the future using light: A review on photocrosslinking reactions, photoreactive groups, and photoinitiators". In: *SLAS Technology* 28.3 (June 2023), pp. 142–151. ISSN: 24726303. DOI: 10.1016/j.slast.2023.02.003.

[18] CELLINK. *Specification sheet GelMA C*. July 2021. URL: https://www.cellink.com/wp-content/uploads/2022/03/Specification-Sheet-GelMA-C_07-July-2021-7.pdf.

[19] CELLINK. *Specification sheet GelMA*. Apr. 2021. URL: https://www.cellink.com/wp-content/uploads/2022/03/Specification-Sheet-GelMA-Bioink-LAP-0.25_08-Apr-2021-1-4.pdf.

[20] CELLINK. *Specification sheet GelXA*. Apr. 2021. URL: https://www.cellink.com/wp-content/uploads/2022/03/Specification-sheet-GelXA_08-Apr-2021-4.pdf.

[21] Yufan Liu et al. "Stiffness-mediated mesenchymal stem cell fate decision in 3D-bioprinted hydrogels". In: *Burns & Trauma* 8 (Jan. 2020). ISSN: 2321-3876. DOI: 10.1093/burnst/tkaa029.

[22] Qiang Wang, Aimin Shi, and Faisal Shah. "Rheology instruments for food quality evaluation". In: *Evaluation Technologies for Food Quality*. Elsevier, 2019. Chap. 18, pp. 465–490. DOI: 10.1016/B978-0-12-814217-2.00018-4.

[23] Kevin Whitcomb. *Determining the Linear Viscoelastic Region in Oscillatory Measurements*. URL: https://www.tainstruments.com/pdf/literature/RH107.pdf.

[24] Bruce Alberts et al. *Molecular Biology of the Cell*. 6th ed. Garland Science, 2015. ISBN: 978-0-8153-4464-3.

[25] Sigma-Aldrich. *Live/Dead Cell Double Staining Kit*. URL: https://www.sigmaaldrich.com/SE/en/product/sigma/04511.

[26] Molecular Probes Inc. *Hoechst Stains*. 2005. URL: https://www.thermofisher.com/document-connect/document-connect.html?url=https://assets.thermofisher.com/TFS-Assets%2FLSG%2Fmanuals%2Fmp21486.pdf.

[27] ThermoFisher Scientific. *ActinGreen™ 488 ReadyProbes™ Reagent (AlexaFluor™ 488 phalloidin)*. URL: https://www.thermofisher.com/order/catalog/product/R37110.

[28] ThermoFisher Scientific. *NucBlue™ Fixed Cell ReadyProbes™ Reagent (DAPI)*. URL: https://www.thermofisher.com/order/catalog/product/R37606.

[29] Bae Lee et al. "Synthesis and Characterization of Types A and B Gelatin Methacryloyl for Bioink Applications". In: *Materials* 9.10 (Sept. 2016), p. 797. ISSN: 1996-1944. DOI: 10.3390/ma9100797.

[30] Matthew G. Haugh et al. "Investigating the interplay between substrate stiffness and ligand chemistry in directing mesenchymal stem cell differentiation within 3D macro-porous substrates". In: *Biomaterials* 171 (July 2018), pp. 23–33. ISSN: 01429612. DOI: 10.1016/j.biomaterials.2018.04.026.

[31] Adam J. Engler et al. "Matrix Elasticity Directs Stem Cell Lineage Specification". In: *Cell* 126.4 (Aug. 2006), pp. 677–689. ISSN: 00928674. DOI: 10.1016/j.cell.2006.06.044.

[32] Amin GhavamiNejad et al. "Crosslinking Strategies for 3D Bioprinting of Polymeric Hydrogels." In: *Small (Weinheim an der Bergstrasse, Germany)* 16.35 (Sept. 2020). ISSN: 1613-6829. DOI: 10.1002/smll.202002931.

[33] John L Farber. "The Role of Calcium Ions in Toxic Cell Injury". In: *Environmental Health Perspectives* 84 (1990), pp. 107–111.

[34] Mikhail A. Grachev, Vadim V. Annenkov, and Yelena V. Likhoshway. "Silicon nanotechnologies of pigmented heterokonts". In: *BioEssays* 30.4 (Apr. 2008), pp. 328–337. ISSN: 02659247. DOI: 10.1002/bies.20731.

[35] Zhou Jian et al. "3D bioprinting of a biomimetic meniscal scaffold for application in tissue engineering". In: *Bioactive Materials* 6.6 (June 2021), pp. 1711–1726. ISSN: 2452199X. DOI: 10.1016/j.bioactmat.2020.11.027.

[36] ThermoFisher. *PrestoBlue™ Cell Viability Reagent*. URL: https://www.thermofisher.com/order/catalog/product/A13261.

[37] Qian Da et al. "Quantifying the cell morphology and predicting biological behavior of signet ring cell carcinoma using deep learning". In: *Scientific Reports* 12.1 (Jan. 2022), p. 183. ISSN: 2045-2322. DOI: 10.1038/s41598-021-03984-4.

[38] Elaheh Alizadeh et al. "TISMorph: A tool to quantify texture, irregularity and spreading of single cells". In: *PLOS ONE* 14.6 (June 2019), e0217346. ISSN: 1932-6203. DOI: 10.1371/journal.pone.0217346.

A

Method development for rheological measurements

A.1 Oscillation time sweep for in situ crosslinking

Since the in situ photo-crosslinking setup was brought into use when the measurements for the initial stiffness testing of this project was conducted, a method testing and development phase had to be performed in order to establish suitable methods. This included how to perform the in situ photo-crosslinking to simulate the conditions of bioprinting, which method settings to use as well as how to measure the change from non-crosslinked bioink to crosslinked bioink. The samples' viscoelastic properties change drastically during the photo-crosslinking in the oscillation time sweep measurement, from a viscous gel with a low storage modulus to a more solid construct with a high storage modulus. To be able to generate stable measurements, different settings were tested and evaluated.

A.1.1 Simulating the conditions of bioprinting

The point of in situ photo-crosslinking is to mimic how the crosslinking is done in the bioprinter in order to measure stiffnesses similar to what can be achieved in a bioprinting experiment. How the bioink is handled right before and after being printed has an impact on how stiff the resulting sample becomes. All photo-crosslinkable bioinks used in this study are gelMA based, making them temperature dependent, which needs to be considered. The general protocol for printing is to first heat up the bioink to 37 °C, followed by letting it equilibrate in a temperature controlled printhead at its specific printing temperature. Using a cooled printbed, the sample is thermally crosslinked right after it has been printed, followed by the photo-crosslinking. All these steps should be taken into account in the in situ crosslinking.

To investigate the conditions the bioink experiences, a test where water was used to simulate the bioink was performed. A cartridge filled with water was placed in a temperature controlled printhead set to 26 °C and left to equilibrate for 30 min. A few drops of water was then extruded into a plastic well plate placed on the printbed, which was set to 15 °C. A thermometer was used to measure the water's temperature right after being extruded into the well, and in the following 1-2 min, to cover the time it could take to print a relatively small construct. The temperature decreased from around 24 °C at the start to 21-22 °C after 2 min. This makes it

evident that the conduction from the printbed to a plastic well plate is not that efficient, and that the temperature set on the printbed does not correspond to the actual temperature of a sample in the well plate.

The chosen sampling procedure used for the rheology measurements of the in situ photo-crosslinking was to heat the bioink at 37 °C for a minimum of 15 min before transferring it to the UPP, which was set to the printing temperature of respective bioink. As the sample volume in this case is significantly smaller, between 160 and 180 µl, compared to a cartridge containing 1-3 ml bioink, 5 min equilibration time at the printing temperature was estimated to be enough. The temperature was then changed to 21 °C, simulating the temperature that the sample is crosslinked at in the bioprinter. After 2 min, the light was switched on to initiate the crosslinking. The stiffness, i.e., the storage modulus, was measured throughout the whole time sweep.

A.1.2 Measurement settings

A setting on the rheometer called "Controlled strain type" determines how each data point is sampled. The option "Precision sampling" was tested but showed to give quite unstable data points thought the whole measurement, and also did not give data points in even intervals as seen in Figure A.1. Analyzing the quality of the data points by evaluating the alignment of the torque and displacement showed a bad alignment. An example of a data point measured with "Precision sampling" can be seen in Figure A.2.

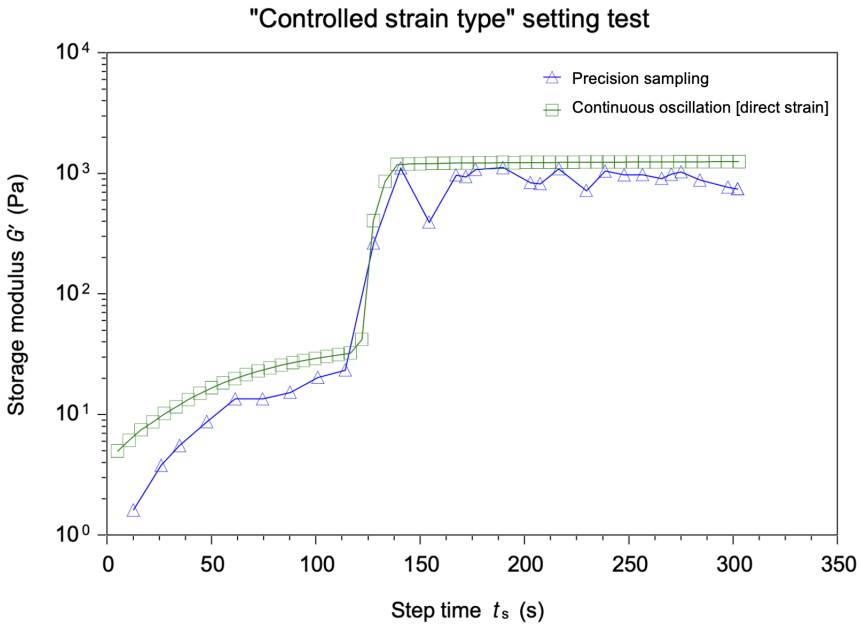

Figure A.1: Test showing the difference between the two settings "Precision sampling" and "Continuous oscillation [direct strain]" in oscillation time sweep measurements.

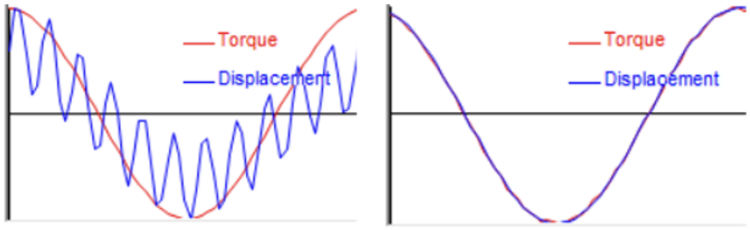

Figure A.2: The torque and displacement alignment for individual data points. To the left showing a data point where the setting "Precision sampling" was used, and to the right showing a data point where the setting "Continuous oscillation [direct strain]" was used.

Using the "Continuous oscillation [direct strain]" option was also tested. The data points generated turned out more stable and in an even distribution throughout the whole measurement, as seen in an example in Figure A.1. Looking at the torque and displacement alignment for the data points, it is also clear that the alignment is much better, as seen in Figure A.2. This setting was therefore selected to be used for all following oscillatory measurements. Another setting that was used for the in situ crosslinking measurements was "Active force control" which aimed to compensate for the samples shrinking in volume after being crosslinked. Using the force control, the measuring gap was automatically adjusted throughout the run to ensure proper surface contact.

A.2 Frequency sweep for pre-crosslinked samples

Measuring already crosslinked samples in the rheometer comes with several challenges to make sure the sample surface has good and even contact with the measuring geometry. It is also important that the sample covers the whole geometry area, meaning these have to be of the same size. Since the sample is solid in this case, it is not possible to trim the sample before starting the measurement. Different methods for producing suitable pre-crosslinked samples were tested, and are described below.

A.2.1 Sample preparation using mold

For previous projects involving ionic crosslinking a mold, seen in Figure A.3, had been used to manually prepare the samples. The mold consists of round wells with a diameter of 8 mm, matching the measuring geometry to be used in this case, in which non-crosslinked bioink was placed. The surface was evened out using a spatula and then the whole plastic mold was submerged in ionic crosslinking solution for a desired amount of time. After a few minutes, when the sample had started to get some shape, a small acupuncture needle was used to cut around the sample's edge to make it release from the mold. After the crosslinking was completed, it was carefully transferred to the rheometer using a spatula. If samples were not measured immediately, they were stored in HBSS (+/+) for up to 30 min.

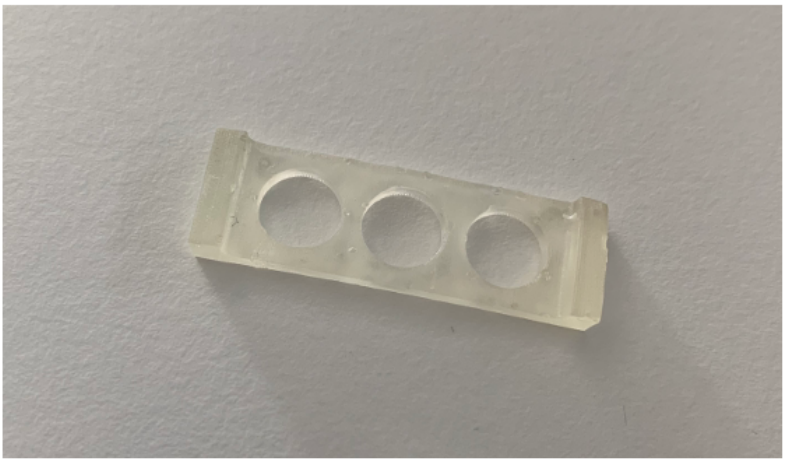

Figure A.3: Mold used for preparing samples pre-crosslinked ionically.

However, samples prepared with this method showed large variation in their surface shape and evenness. The process was also time-consuming and did not allow preparation of a large number of samples at the same time. Furthermore, it could only be used to prepare ionically crosslinked samples and not samples requiring photo-crosslinking. Therefore, other options for preparing pre-crosslinked samples were investigated.

A.2.2 Sample preparation using 3D bioprinting

The, in some aspects rather obvious, option of using 3D bioprinting for printing and crosslinking the samples was investigated as this would hopefully generate more reproducible samples compared to a method with quite a few manual steps. A model of disk with 8 mm diameter and a height of 0.5 mm was created as an stl-file to be used in the bioprinter. Different grades of infill density were tested, and it was observed that 43 % infill density generated a dense disk with a more even surface compared to the ones prepared using the mold.

A.2.3 Surface contact and axial force test

When measuring pre-crosslinked samples, one cannot ensure good surface contact with the measuring geometry by always using the same measuring gap and and trimming off any excess material, as one can in the case with non-crosslinked samples. Even though sample height can be controlled in the model used by the printer, other factors like nozzle size and bioink viscosity contribute to the final shape and height of the sample, which turned out to give a some variation between samples, especially when comparing different bioinks.

To avoid compressing and breaking samples being slightly too high, and not getting proper surface contact with samples being slightly too low, the measuring gap was

instead determined based on the value of the axial force experienced by the measuring geometry. This real-time value is displayed also before starting a measurement, which allowed the measuring geometry to be lowered down towards the sample carefully until reaching a certain axial force, ensuring proper surface contact, and then starting the measurement. The axial force which had previously been used for similar measurements in other projects, on samples prepared with the mold, was 0.1 N. This axial force was tested on some samples of CELLINK Bioink to investigate if it could be a suitable value to use also in this case. Some results can be seen in Table A.1. The results were more reproducible compared to the results obtained when preparing the samples using the mold.

Table A.1: Stiffnesses measured for printed and pre-crosslinked samples of CELLINK Bioink using an axial force of 0.1N.

Sample	**CELLINK 10 min 50 mM**	**CELLINK 2 h 10 mM**
1	12 499 Pa	7 986 Pa
2	13 434 Pa	7 442 Pa
3	14 208 Pa	8 908 Pa

A.2.4 Sandblasted or cross hatched geometry

For the initial stiffness testing, a cross hatched 8 mm geometry was used for the pre-crosslinked samples. A concern was, however, that the relatively large serrations on the geometry's surface could lead to a higher observed axial force for stiffer samples before the geometry was in proper contact with the whole sample surface. Sometimes, the small spikes would also leave dents in softer samples after a measurement, potentially destroying it. The possibility of instead using a geometry with a smoother surface, more like the smooth UPP 20 mm one, was therefore investigated. A sand blasted 8 mm geometry could eventually be borrowed and compared to the cross hatched one with regards to variability between samples. Both geometries can be seen in Figure A.4.

Figure A.4: Cross hatched (left) and sand blasted (right) geometry.

For comparison, printed 8 mm GelXA disks of two different crosslinking conditions were used and measured with both geometries. All measurements were started at 0.1 N axial force, measured at 0.5 Hz and 0.1 % strain. The results from the measurements are seen in Table A.2 and Table A.3.

Table A.2: A comparison of stiffnesses of GelXA disks when photo-crosslinked for 5 s, measured with the cross hatched and the sand blasted geometry.

Sample	**Cross hatched**	**Sand blasted**
1	1 915 Pa	1 458 Pa
2	1 245 Pa	1 406 Pa
3	1 000 Pa	1 307 Pa

Table A.3: A comparison of stiffnesses of GelXA disks when photo-crosslinked for 15 s, measured with the cross hatched and the sand blasted geometry.

Sample	**Cross hatched**	**Sand blasted**
1	1 455 Pa	2 090 Pa
2	1 082 Pa	1 918 Pa
3	1 079 Pa	1 809 Pa

The stiffnesses measured with the sand blasted geometry showed slightly less variation between the three samples in both cases, compared to the cross hatched one. The samples crosslinked for 15 s are also measured to be stiffer than the ones crosslinked for only 5 s when using the sand blasted geometry. This correspond to the principle the longer exposure to light leads to a higher degree of crosslinking. With the cross hatched geometry, on the other hand, the stiffness values for both 5 s and 15 s varied between approximately 1000 and 1500-2000 Pa. The mean stiffness for 5 s photo-crosslinking is 1 387 Pa and the mean stiffness for 15 s photo-crosslinking is 1 205 Pa, which makes it hard to conclude if there actually is a difference between the two conditions. Although this comparison only included a small number of samples of one type of bioink, making it hard to make any definite conclusions about which measuring geometry would be more suitable for these types of samples and measurements, the sand blasted one was chosen to be used in all future measurements. The fact that it is more similar to the smooth UPP 20 mm also makes the different measurements more comparable.

B

Viability data for day 14

As described previously, the viability data for day 14 was excluded form the results due to difficulties in the analysis. In Figure B.1, an example of microscopy images for GelMA 5 s photoX at day 14 can be seen.

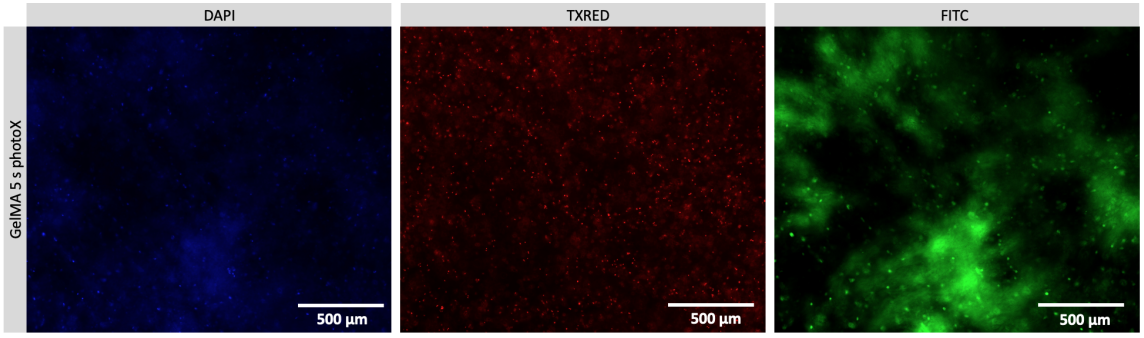

Figure B.1: Microscopy images showing the three analyzed channels of the viability staining at day 14. The sample shown is GelMA 5 s photoX.

As seen in Figure B.1, it is difficult to distinguish all individual cells using the Hoechst staining in the DAPI channel. There is some background fluorescence covering some areas of the image, and the cells are not very brightly fluorescent. As Hoechst is supposed to stain the nuclei of all cells, both live and dead, the aim was to count these cells and use it as the total number of cells in the sample. The dead cells, stained with PI as seen in the TXRED channel, were then subtracted from the total number of cells. However, since the PI staining gives a stronger fluorescence for the cells, these were easier to count and resulted in a high dead cell number. When calculating the percentage of viable cells, the viability then became negative as more dead cells were counted compered to the total number of cells. A negative viability is not possible, and as seen in the FITC channel, some viable cells are present in the sample as well.

This problem with a negative viability occurred for one or two samples in a few of the bioinks at day 14. For the majority of the samples, a positive viability percentage was obtained, but the images were still quite difficult to analyze, making the reliability of the results questionable. Presenting the day 14 viability for the bioinks and conditions that did not result in negative values could have been an option, but due to the concerns regarding reliability of these as well, it was decided to exclude all the day 14 results. Another possibility would have been to count the

live and dead cells based on the FITC and the TXRED channel, as was done at day 1 and day 7, but due to time restrictions it was not possible to repeat the whole analysis process. Furthermore, the fluorescent signal in the FITC channel was of varying intensity and for some bioinks and conditions, individual cells would have been difficult to distinguish due to the spreading of the cells occurring at this stage of the experiment. Suggestions for how to successfully analyze the cell viability for later time points is included in the "Improvements and future research" section of the Results and Discussion.

DEPARTMENT OF PHYSICS
CHALMERS UNIVERSITY OF TECHNOLOGY
Gothenburg, Sweden
www.chalmers.se

CHALMERS
UNIVERSITY OF TECHNOLOGY